

# **Guitar Amplifier Identification Through Digital Signal Processing Techniques**

Stephen Blackmore

Submitted in partial fulfillment of the requirements for the  
Master of Music in Music Technology

Department of Music and Performing Arts Professions

The Steinhardt School

New York University

Advisor: Dr. Agnieszka Roginska

Submitted April 29, 2013

## Acknowledgements

I would first like to thank Amanda Garfield for her encouragement to focus on what I wanted and apply to graduate school in the first place, her willingness to move to New York City with me, and her love and support throughout this whole process. I could not have done any of this without her.

I would like to say a special thanks to Aron Glennon for his advice and assistance. Thank you to Jim Aveni for being a cool dude and for providing all of the guitar samples used in this thesis. Thanks to Justin Matthew for helping me get the amplifier data together and helping me get started, and thank you to Cheng-I Wang, Don Bosley, and Andrew Madden for talking through some of the finer points of approach and analysis with me. Thank you to Dr. Mark Ericson at the Army Research Lab for his mentorship and willingness to discuss ideas with me.

Finally, thank you to Dr. Roginska for helping me to arrive at this topic and providing invaluable advice along the way.

# Table of Contents

<b>ABSTRACT .....</b>	<b>1</b>
<b>1. INTRODUCTION.....</b>	<b>2</b>
1.1. ACOUSTIC SIGNATURE AND AUDIO FINGERPRINTING .....	2
1.2. MUSICALLY APPLIED ACOUSTIC SIGNATURE.....	3
1.3. OBJECTIVE.....	4
1.4. APPLICATIONS.....	5
<b>2. BACKGROUND.....</b>	<b>6</b>
2.1. ACOUSTIC SIGNATURE APPLICATIONS .....	6
2.2. IDENTIFICATION OF MUSICAL INSTRUMENTS.....	7
2.3. METHODOLOGY AND DATA ANALYSIS FOUNDATION.....	11
<b>3. METHODOLOGY .....</b>	<b>13</b>
3.1. OVERVIEW .....	13
3.2. DATA COLLECTION .....	14
3.3. PRE-PROCESSING: AMPLIFIER DATA PREPARATION.....	15
3.4. PRE-PROCESSING: CONVOLUTION AND DECONVOLUTION.....	19
3.4.1. <i>Convolution</i> .....	19
3.4.2. <i>Deconvolution</i> .....	21
3.5. POST-PROCESSING ANALYSIS .....	24
3.5.1. <i>Listening test performed on training data</i> .....	24
3.5.2. <i>Octave band filtering on training data</i> .....	25
3.5.3. <i>Octave band filter results storage</i> .....	25

3.5.4. Principal component analysis (PCA) data preparation.....	27
3.5.5. PCA processing.....	28
3.6. IDENTIFICATION .....	29
3.6.1. Method One: comparison of test data against training data .....	29
3.6.2. Method Two: comparison of test data against itself.....	30
3.6.3. Measuring precision .....	31
<b>4. RESULTS .....</b>	<b>33</b>
4.1. DECONVOLUTION RESULTS.....	33
4.2. TRAINING DATA RESULTS (METHOD ONE) .....	38
4.3. TESTING DATA RESULTS (METHOD Two).....	45
<b>5. DISCUSSION .....</b>	<b>54</b>
5.1. TRAINING DATA RESULTS SERVED AS A DISCOVERY METHOD .....	54
5.2. LINEARITY AS DECIDING FACTOR.....	55
5.3. IDENTIFICATION IS BASED ON INDIVIDUAL OUTPUT; NOT A SECONDARY DATA SET .....	56
5.4. DEGREE OF DATA FILTERING AFFECTS ACCURACY .....	57
<b>6. CONCLUSIONS AND FUTURE WORK .....</b>	<b>59</b>
<b>7. WORKS REFERENCED.....</b>	<b>62</b>
<b>APPENDIX.....</b>	<b>64</b>
7.1. SPECTRAL PLOTS OF FACE PLANE OUTPUTS .....	64
7.2. CODE FOR BEST-FIT LINE AND DISTANCE CALCULATION .....	71

## Figures and Tables

FIGURE 3.1-1 OUTLINE OF METHODS FROM DATA COLLECTION, SIGNAL PROCESSING, TO AMPLIFIER IDENTIFICATION	13
FIGURE 3.3-1 THE DIMENSIONS OF THE AMPLIFIERS OUTLINED IN BLACK OVERLAIDED WITH THE GRID OF MICROPHONE ARRAY CAPSULES IN THE FACE PLANE MEASUREMENT GRID (MATTHEW, 2012)	17
FIGURE 3.3-2 OUTLINE OF HOW THE AMPLIFIER CENTERS WERE DETERMINED. THE DOTTED LINE IN THE GREY SQUARE REPRESENTS THE CENTERED AREA OF THE FENDER DELUXE. THE MOVING WINDOW MOVES ACROSS THE GRID (THE RED SQUARE) THROUGH ALL COLUMN INDICES AND THEN DOWN ONE ROW (THE BLUE SQUARE), AND REPEATS THROUGH ALL POSITIONS. THE RESULTS ARE STORED, AND THE 7X7 GRIDS ON EACH OF THE OTHER TWO AMPLIFIERS WHERE THE ABSOLUTE VALUE OF THE STANDARD DEVIATION WAS LOWEST WERE USED AS THE CENTERS OF THE AMPLIFIERS.	19
FIGURE 3.4-1 PROCESSING STEPS FOR THE CONVOLUTIONS/DECONVOLUTION PROCESSES	23
FIGURE 3.5-1 OVERVIEW OF HOW DATA WAS ORGANIZED AND STORED FOR THE FILTERED DECONVOLUTIONS. THE THREE DECONVOLUTION ARRAYS (ONE FOR EACH AMPLIFIER) FOR EACH OF THE OCTAVE BAND FILTERS WAS STORED IN THE SAME WAY.	26
FIGURE 4.1-1 DECONVOLUTIONS FROM THE RAEZER'S EDGE DECONVOLUTION ARRAY ACROSS 6 OCTAVES OF F. THE RAEZER'S EDGE WAS THE CORRECT DECONVOLUTION HERE, AND THE OTHER TWO AMPLIFIERS WERE INCORRECT. THE RAEZER'S EDGE IS THE TOP AMPLIFIER IN EACH OF THE SIX PLOTS.	34
FIGURE 4.1-2 DECONVOLUTIONS FROM THE FENDER DELUXE DECONVOLUTION ARRAY ACROSS 6 OCTAVES OF F. IN THIS EXAMPLE, THE DELUXE WAS THE CORRECT DECONVOLUTION, AND THE OTHER TWO AMPLIFIERS WERE INCORRECT. THE DELUXE IS THE MIDDLE AMPLIFIER IN EACH OF THE SIX PLOTS.	35
FIGURE 4.1-3 DECONVOLUTIONS FROM THE VOX VALVETRONIX DECONVOLUTION ARRAY ACROSS 6 OCTAVES OF F. IN THIS EXAMPLE, THE VOX WAS THE CORRECT DECONVOLUTION, AND THE OTHER TWO AMPLIFIERS WERE INCORRECT. THE VOX IS THE BOTTOM AMPLIFIER IN EACH OF THE SIX PLOTS.	36
FIGURE 4.2-1 PLOT OF FIRST THREE PRINCIPAL COMPONENTS OBTAINED FROM PCA FILTERED WITH 1/12TH OCTAVE BANDS	39
FIGURE 4.2-2 FIRST THREE PRINCIPAL COMPONENTS, CORRECT DECONVOLUTIONS ONLY, FILTERED THROUGH 1/12TH OCTAVE BANDS, WITH LINE OF BEST FIT OVERLAID	39
FIGURE 4.2-3 PLOT OF FIRST THREE PRINCIPAL COMPONENTS OBTAINED FROM PCA FILTERED WITH 1/6TH OCTAVE BANDS	40
FIGURE 4.2-4 FIRST THREE PRINCIPAL COMPONENTS, CORRECT DECONVOLUTIONS ONLY, FILTERED THROUGH 1/6TH OCTAVE BANDS, WITH LINE OF BEST FIT OVERLAID	41

FIGURE 4.2-5 PLOT OF FIRST THREE PRINCIPAL COMPONENTS OBTAINED FROM PCA FILTERED WITH 1/3RD OCTAVE BANDS	41
FIGURE 4.2-6 FIRST THREE PRINCIPAL COMPONENTS, CORRECT DECONVOLUTIONS ONLY, FILTERED THROUGH 1/3RD OCTAVE BANDS, WITH LINE OF BEST FIT OVERLAI	42
FIGURE 4.3-1 ONE-THIRD OCTAVE FILTERED OF TEST SAMPLE DECONVOLUTIONS WITH LINES OF BEST FIT	46
FIGURE 4.3-2 ONE-SIXTH OCTAVE FILTERED DECONVOLUTIONS OF TEST SAMPLE WITH LINES OF BEST FIT	47
FIGURE 4.3-3 ONE-TWELFTH OCTAVE FILTERED DECONVOLUTIONS OF TEST SAMPLE WITH LINES OF BEST FIT	47
FIGURE 7.1-1 DECONVOLUTIONS FROM THE RAEZER'S EDGE DECONVOLUTION ARRAY ACROSS 6 OCTAVES OF A. IN THIS EXAMPLE, THE RAEZER'S EDGE WAS THE CORRECT DECONVOLUTION, AND THE OTHER TWO AMPLIFIERS WERE INCORRECT. THE RAEZER'S EDGE IS THE MIDDLE AMPLIFIER IN EACH OF THE SIX PLOTS.	65
FIGURE 7.1-2 DECONVOLUTIONS FROM THE RAEZER'S EDGE DECONVOLUTION ARRAY ACROSS 6 OCTAVES OF C. IN THIS EXAMPLE, THE RAEZER'S EDGE WAS THE CORRECT DECONVOLUTION, AND THE OTHER TWO AMPLIFIERS WERE INCORRECT. THE RAEZER'S EDGE IS THE MIDDLE AMPLIFIER IN EACH OF THE SIX PLOTS.	66
FIGURE 7.1-3 DECONVOLUTIONS FROM THE FENDER DELUXE DECONVOLUTION ARRAY ACROSS 6 OCTAVES OF A. IN THIS EXAMPLE, THE DELUXE WAS THE CORRECT DECONVOLUTION, AND THE OTHER TWO AMPLIFIERS WERE INCORRECT. THE DELUXE IS THE MIDDLE AMPLIFIER IN EACH OF THE SIX PLOTS.	67
FIGURE 7.1-4 DECONVOLUTIONS FROM THE FENDER DELUXE DECONVOLUTION ARRAY ACROSS 6 OCTAVES OF C. IN THIS EXAMPLE, THE DELUXE WAS THE CORRECT DECONVOLUTION, AND THE OTHER TWO AMPLIFIERS WERE INCORRECT. THE DELUXE IS THE MIDDLE AMPLIFIER IN EACH OF THE SIX PLOTS.	68
FIGURE 7.1-5 DECONVOLUTIONS FROM THE VOX VALVETRONIX DECONVOLUTION ARRAY ACROSS 6 OCTAVES OF A. IN THIS EXAMPLE, THE VOX WAS THE CORRECT DECONVOLUTION, AND THE OTHER TWO AMPLIFIERS WERE INCORRECT. THE VOX IS THE MIDDLE AMPLIFIER IN EACH OF THE SIX PLOTS.	69
FIGURE 7.1-6 DECONVOLUTIONS FROM THE VOX VALVETRONIX DECONVOLUTION ARRAY ACROSS 6 OCTAVES OF C. IN THIS EXAMPLE, THE VOX WAS THE CORRECT DECONVOLUTION, AND THE OTHER TWO AMPLIFIERS WERE INCORRECT. THE VOX IS THE MIDDLE AMPLIFIER IN EACH OF THE SIX PLOTS.	70

## Abstract

This thesis tests whether differing acoustic signatures between amplifiers can be used to identify individual amplifier models in recorded performances. Utilizing a training set of impulse responses from three unique guitar amplifier models, data is passed through a process of convolution, deconvolution, octave band filtering, and principal component analysis. Analysis defined the acoustic signature as a differentiating pattern between correctly and incorrectly deconvolved signals. Two methods are presented for amplifier identification. The first method uses a test set of guitar signals where no information about the input signal is known and compares it against a training data set of guitar signals, and an attempt is made to identify the amplifiers based on their acoustic signature. The second method uses only information obtained from each test signal to identify amplifiers.

The results of the second method showed an accurate identification of which amplifier was recorded, and this differentiation and classification can be performed on music signals even when the original, un-convolved signal is unknown.

# **1. Introduction**

Many musicians claim that they can determine the brand of an instrument by its sound alone. This thesis seeks to study programmatically what these musicians know intuitively and will test whether a particular brand of guitar amplifier can be identified with reliable accuracy from a recorded performance. Despite extensive research in the field of instrument classification using varied techniques, very little research has focused on differentiating models or brands of the same instrument.

## **1.1. Acoustic signature and audio fingerprinting**

An identifiable and unique sound is described by its “Acoustic signature” -- an umbrella term that encompasses every aspect of a sound that makes it unique and identifiable. The impulse response, spectral content, modulation envelope, and many other such features are the components of an audio source’s acoustic signature. The ability to identify and quantify differences in sound output is crucial in numerous applications such as music, the military, and many natural science fields. This identification is enabled by digital signal processing techniques.

Acoustic signature identification involves processes that isolate the different components of a source’s sound output. Audio fingerprinting is the process of using a source’s acoustic signature for identification or to extract information about the source. Factors such as shape, size, component materials, and construction techniques strongly influence the sound output of a source by changing aspects of the audio fingerprint such as the timbre, spectral content, and envelope. These sonic characteristics vary greatly in their

significance in the audio fingerprint and one must identify which are the most important to efficiently identify a sound's source. One of these factors is the impulse response, which will be measured in this thesis for different guitar amplifiers.

## **1.2. Musically applied acoustic signature**

Just like any other audio source, one class of musical instruments' sound is unique when compared to a different class (e.g., piano versus trombone). In most cases, the sound of one instrument playing a particular pitch will differ from another instrument playing the same pitch and often can be identified by ear. This difference is sometimes referred to as the instrument's timbre. Much work has focused on the differentiation and identification of instrument classes using measures of timbre such as Mel Frequency Cepstral Coefficients (MFCCs) (e.g., (Logan, 2000)(Brown, Houix, McAdams, 2001) (Eronen and Klapuri, 2000)). With these measurement techniques it becomes reasonably simple to differentiate a piano from a violin. However, these techniques cannot reliably differentiate different models or brands of the same class of instrument such as a Steinway piano versus a Bösendorfer piano.

Many musicians claim that they are able to discern the sound of one particular model of an instrument from another—an ability that has been studied (Fritz, Curtin, Poitevineau, Morrel-Samuel, Tao, 2011). Outside of the musical realm, humans are able to identify the make and model of other sound sources such as cars, helicopters, and airplanes. This innate ability suggests that there exist features within the sound of any given model of object or instrument that are technically unique and identifiable through measurement and analysis.

### **1.3. Objective**

The research in this thesis utilizes impulse responses from three unique guitar amplifier models to convolve with guitar signals. A test set where no information about the input signal is known is compared against a training set and also against itself, and an attempt is made to identify the amplifiers based on their acoustic signature. The objective of this study is to determine if differing acoustic signatures between amplifiers can be used to identify individual amplifier models used in recorded performances.

Guitar amplifiers are used as the instrument for this study because they are an essential tool in the arsenal of musicians and recording engineers. Different guitar amplifier models are used in varying configurations to achieve certain desired tones and coloration in both live and recorded musical performances, producing the final output sound for electric guitars.

The impulse response measurements of three guitar amplifier models will be compared to demonstrate differences across an area around the center of the speaker. The impulse response will then be used for convolution with samples from an electric guitar performing short musical excerpts. The convolved signals will be processed through deconvolutions, filtering, and Principal Component Analysis. The final goal of processing is to determine probabilistically which of the amplifiers was used to create a recorded output sound without prior knowledge of the input signal before convolution.

Humans cannot always differentiate models and brands of the same instrument. This inability highlights one of the more difficult challenges of model classification based solely on recorded sound; any signal processing approach will necessarily suffer from varying degrees of uncertainty. For this reason, this study will not seek to verify absolutely which

guitar amplifier model was used for a recorded performance. Instead, percentages of certainty will be calculated to identify which amplifier model was most likely used for the recording.

#### **1.4. Applications**

The determination of an instrument's make and model based on a recorded output would prove useful to musicians, audio engineers, and recording artists. The methods described in this thesis could identify which particular model of instrument would produce the desired sound. With expanded research based on the methods in this thesis, additional determinations could be made about the spatial relationships of instrument placement. This research could be applied to provide recording professionals with powerful tools to achieve creative goals by informing decisions on instrument selection based on desired sonic characteristics from previously recorded material.

This thesis tests whether differing acoustic signatures between amplifiers can be used to identify individual amplifier models in recorded performances. Impulse responses from three unique guitar amplifier models are passed through a process of convolution, deconvolution, octave band filtering, and principal component analysis. Two methods for amplifier identification are then presented, and the results of each method will be analyzed and compared.

## **2. Background**

### **2.1. Acoustic signature applications**

The acoustic signature at a basic level is the set of acoustic patterns emitted from a source. It describes the factors that give a system a defined and identifiable overall sound in much the same way that timbre describes how human beings identify different musical instruments.

Acoustic signatures are widely used to identify various information sources such as seismic events (Whalen, 1971), the human voice (Rabiner and Schafer, 1978), or electro-mechanical objects such as ships, submarines, airplanes, helicopters, and other such vehicles (Mairaj, 2011). Ongoing research at the U.S. Army Research Laboratory at Aberdeen Proving Ground in Maryland is utilizing these processes to identify helicopters. Their unpublished study seeks to identify the components in helicopter sounds that allow humans to detect, localize, and determine the type of helicopter they are hearing.

The author of this thesis was part of the research team on the Army's project, working on modulation envelope extraction and analysis. This Army study also seeks to determine how humans can differentiate between makes and models of sound sources. The objective of that study served as a basis for researching musical instrument brand identification using similar techniques for this thesis.

Other researchers have also used acoustic signature analysis and audio fingerprinting for detection/identification of specific military versus civilian aircraft (Mairaj, 2011). Mairaj describes a system for the detection and identification of aircraft, using the Energy Spectral Density (ESD) as the main feature in a feature space. He uses Euclidean distance of

measured ESD compared to the feature space to identify aircraft (Mairaj, 2011). The identification of naval warships has also been tested using acoustic signature analysis. Filinger, Sutin, and Sedunov (2010) use cross-correlation methods to identify the acoustic signatures of moving naval ships.

Many of the same acoustic signature analysis techniques used in the military and natural sciences can be extended to the realm of musical instruments. In addition to measures of timbre, musical instruments possess unique radiation patterns and spectral characteristics. As described in Roginska, Case, Madden, and Anderson (2011), many studies have focused on the radiation pattern differences between classical musical instruments. This thesis serves as an extension of the work by Roginska, et al., (2012) by taking many of the same measurements and the trends observed from radiation pattern analysis and using that information to determine the output source.

## **2.2. Identification of musical instruments**

No published literature was found about research identifying instrument models or brands within a class through analysis of sound data. This thesis seeks to contribute a method of instrument model identification through data analysis; however, some studies of identification through human perception have been used to inform the author's investigation.

There have been numerous studies about instrument class identification through human perception. It has been shown that humans are able to differentiate between classes of instruments (e.g., a violin versus a piano playing the same pitch) as well as to distinguish multiple sources in an auditory stream (i.e., "whether a sequence of acoustic

events results from one, or more than one, ‘source’” (McAdams and Bregman, 1979))(Patil, Pressnitzer, Shamma, Elhilali, 2012). Many such studies have focused exclusively on timbre and its quantification, and much work has focused on the use of spectral features as tools for the classification of timbre and instrument identification (Logan, 2000)(Brown, Houix, McAdams, 2001) (Eronen and Klapuri, 2000). The examples mentioned are just a few in a vast amount of literature on timbre measurements and instrument identification.

Prior research into how humans can identify specific brands of viscerally perceived stimuli has occurred across all of the human senses – taste, touch, sound, smell, and vision. For example, Plassmann, O’Doherty, Shiv, and Rangel, studied how the price of different wines affected the perception, and they showed that the study subjects’ belief about the price of the wines modulated their perceptions of quality, with higher prices resulting in a perceived higher quality and vice-versa (2008). They also demonstrated the neurological effects in the brain of these perceptions by “scanning subjects using functional MRI while they tasted wines that, contrary to reality, they believed to be different and sold at different prices” (Plassmann, et al., 2008). Their findings suggest that often other, non-visceral attributes play a large role in how we ultimately interpret what our senses perceive.

A full psychological study of why humans tend to allow prior knowledge or biases to affect their senses is outside of the scope of this thesis. Scientifically obtained measurements of physical phenomena will not always solely account for how human beings interpret the data obtained from their senses—they often have prior knowledge or are predisposed to a brand bias (Plassmann, et al., 2008). For example, while one may not be able to identify wine based on taste, a prior knowledge of wine brands or French regions might predispose them towards a specific identification.

These observations are easily extendible to musical instrument identification. Many musicians allow the price or notoriety of a specific instrument brand to modulate their expectations of quality rather than just choosing instruments based on a particular sound they enjoy. Similar findings have also been shown in musical instrument brand and model bias (Fritz, et al., 2011).

Due to the fame and notoriety of the Stradivarius violins, researchers have attempted for many years to quantify exactly what differentiates these violins from other violins and why so many musicians and experts claim that these violins are the best sounding. Theories describing the pre-Ice-Age wood (Burckle and Grissino-Mayer, 2003, qtd. in Fritz, et al., 2011) as a factor to the type of lacquer available at the time (Hill and Hill, 1901, qtd. in Fritz, et. al., 2011)(Schelling, 1968, qtd. in Fritz, et. al., 2011) have been put forward to attest for the desirable qualities of these violins. The prevalence of these studies and their lack of definitive conclusions indicate how perplexing a problem it is to identify why one particular model of instrument is preferred over another by trained musicians.

The study by Fritz, et al., (2011) explores the perception of violins without any knowledge of make and model. In the paper “Player Preferences Among New and Old Violins,” the authors attempt to determine if expert level violinists really can perceive a difference in the sound quality when they are given no other information about the instrument they are playing/hearing. The authors also compare this study to the wine study mentioned previously (Plassmann, et al., 2008). They obtained several levels of violin models that had been ranked as “student,” “decent professional,” and “fine solo instrument” (including Stradivari and Guarni del Gesu models). They used a double-blind method of testing the different models of violin, and they found that the most preferred

models among the professional violinists who participated in this test were newer models, and the least preferred model was the Stradivarius. Most players were unable to tell the age of any of the violins they played, and there was “scant correlation between age/monetary value and perceived quality” (Fritz, et al, 2011).

Their testing methods could be disputed, since all of the tests were performed in a dry-sounding hotel room rather than a concert hall (an environment that the test subjects would be more attuned to). They also used a small sample size of only twenty-one participants (Fritz, et al, 2011). However, the results do suggest that when all other factors are controlled, the sound by itself may not provide enough data on the surface to differentiate between different models of the same instrument.

In 2008, George Bissinger published an in-depth study entitled “Structural Acoustics of Good and Bad Violins” that measured the acoustics of various violins. They asked a panel to rank the violins as ‘good,’ ‘intermediate,’ and ‘bad’ based on their expertise as violinists and luthiers. Included as part of the ‘good’ violins were several Stradivari and Guarni del Gesu models, which are highly regarded by musicians worldwide. The modal-acoustic radiation patterns of these violins were measured involving radiativity, directivity, effective critical frequency, damping, fraction-of-vibrational-energy radiated, and other such data for several models of violin. In almost all features, there was no measurable differentiator between the three levels of violin models. Interestingly, they even found that some of the violins ranked as “good” did not perform as well as the “bad” and “intermediate” in measures of directivity and damping. The only differentiator that seemed consistent across all “good” violins was “an approximately 280 Hz, Helmholtz-type A0 cavity mode radiativity” (Bissinger, 2008). This conclusion indicates that the differences

between models of the same instrument are complex and difficult to measure. However, differences do exist, and it is the goal of this thesis to use the differences for the purpose of identification.

### **2.3. Methodology and data analysis foundation**

This thesis seeks to distinguish guitar amplifiers used for recordings without knowledge of the original input signal. In order to accomplish this task, blind deconvolution was used to separate inputs from the impulse responses of guitar amplifiers. This method has been extensively used in similar studies.

Methods for “blind deconvolution” were first explored and described in the literature with the work of Thomas Stockham (Stockham, 1971)(Stockham, 1975). Stockham sought to recover the original performances of opera singer Enrico Caruso that had been originally recorded to wax cylinders in the early 20<sup>th</sup> century. In “Restoration of Old Acoustic Recordings,” he describes his approach and how he was able to approximate the original signals using deconvolution methods (Stockham, 1971). While the methods presented in this thesis differ in goal and methodology from Stockham’s work, his use of deconvolution for a similar cause informs this paper’s methodology.

Ongoing work at the Music and Audio Research Lab (MARL) at New York University is focused on measuring the spectral characteristics, radiation patterns, and directivity of various guitar amplifier models. Dense measurements around the front, back, sides, and above the Fender Twin Reverb guitar amplifier are presented in (Roginska, et al., 2012) and (Madden, 2012) in order to “gain insight and an understanding of the spectral directivity sensitivity factor of the electric guitar amplifier” (Roginska, et al., 2012). The

vertical plane of the same amplifier using various microphone placement distances is introduced in a follow-up paper (Roginska, Matthew, Madden, Anderson, and Case, 2012).

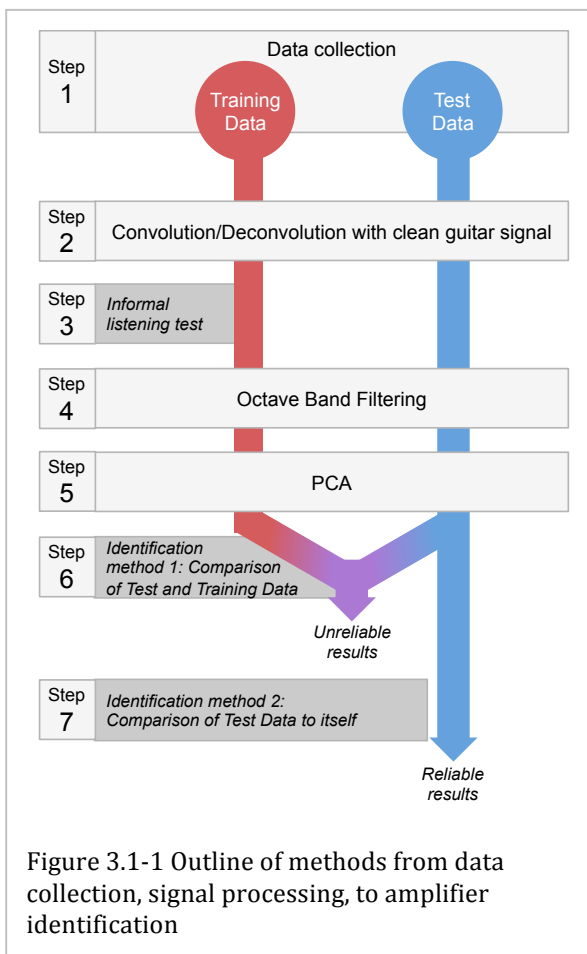
Two other newly measured guitar amplifiers are described in Matthew (2012) and Matthew and Blackmore (2013). The measurement techniques for these additional guitar amplifiers are the same as in the papers mentioned previously, but they serve to increase the data set of densely measured guitar impulse responses. All three densely measured guitar amplifier impulse responses from the studies mentioned above are used in this thesis.

This thesis will employ existing and widely used DSP techniques such as the Discrete Fourier Transform (DFT), convolution, deconvolution, and several types of octave band filters to manipulate a dense data set of guitar amplifier impulse responses, and Principal Component Analysis (PCA) as described by Schiens (2009). Schiens provides an excellent explanation of PCA as a method for dimensionality reduction and the discovery of “simple, underlying structures in complex data sets using analytical solutions from linear algebra” (Schiens, 2009). The data sets resulting from the processing methods in this thesis consisted of many dimensions, and using PCA allows for a reduction of the redundant or extraneous data, allowing for a more narrow focus on the components that allow for amplifier identification.

### 3. Methodology

#### 3.1. Overview

The data for this study was obtained from three different guitar amplifiers. Three sets of guitar data were collected using the same methods and parameters. The first set, or the ‘training set’ established a baseline to measure against. A second set of data, or the ‘testing



set’ would be used to run subsequent tests that the results are based on. The training set and the testing set used the same guitar and performer playing different musical excerpts. The final, smaller set used the same performer using a different guitar and playing different musical excerpts.

After processing the signals, the results were analyzed, and identification of the amplifiers was attempted using two similar but different methods. Finally, the success of each method was measured and compared. This process is outlined in Figure 3.1-1.

### **3.2. Data collection**

The guitar amplifier data for this paper was obtained from several different recording sessions, using the ScanIR system described by Boren and Roginska (2011). The same data obtained by Matthew and Blackmore (2013) is used here, as the author also participated in the collection of that data. Although only three guitar amplifier models were used for this paper, the methodology serves as a prototype for a much larger dataset, involving more measurements and amplifier models.

Since the measurement techniques used have been previously and extensively described, the specific impulse response measurement methodology will not be discussed here (Boren and Roginska, 2011), (Roginska, et. al., 2012), (Matthew and Blackmore, 2013), (Matthew, 2012), (Madden 2012). For this study, only the face plane of the amplifiers was considered with the microphone array at a distance of two inches. The face plane consists of the front of the amplifier in the direction that the speaker faces.

The guitar samples were recorded direct into a MacBook Pro running Pro Tools at a 48 kHz sampling rate with 16-bit resolution. These signals were then bounced to .WAV files, read into Matlab, and stored in 1x10 cell arrays.

The guitar used for all samples in the main training and testing data was a Gibson Les Paul Standard, and no digital audio effects or other processing techniques were applied to the clean signal. Ten short musical snippets of approximately ten seconds each in length were recorded for the training set. The samples included segments of popular songs, arpeggio chords, and scales performed with differing dynamics ranging from mezzo piano to forte.

In addition to the original ten guitar samples used to create the training data, ten additional samples were collected with the same methods, performer, and guitar. These samples were stored in a separate cell array in exactly the same way as the samples were stored for the training data set.

A final small set of test signals was collected from the same performer playing a different guitar. Four short musical samples were collected from the performer using a Fender Telecaster. These samples were recorded in exactly the same way as the samples from the Les Paul. This set was created in a separate, later recording session to provide additional data for testing. This additional data would lend more credence to the amplifier identification results to show that the methods presented in this work are extensible and not dependent on a constrained set of parameters.

### **3.3. Pre-processing: amplifier data preparation**

The three amplifiers used in this study have differing shapes and sizes. In order to compare them to each other, the first necessary step was to determine a constant parameter for measurement across the three models. Comparing face-plane-only measurements was determined through a constant-sized area for each amplifier centered over the cone of the speaker. The center of the speaker was chosen to ensure that the areas of similar audio output power and content were being compared.

The Fender Reverb Deluxe specifications have been well documented in the studies mentioned previously, and physical inspection verified the location of the center of the speaker cone after the impulse response measurement sessions.

In addition to the Fender Deluxe, a Vox Valvetronix VT20+ and a Raezer's Edge Stealth 12 ER cabinet containing a 12" loudspeaker amplified by an Acoustic Image Clarus 2R were measured. These other two amplifiers belonged to private individuals and were not available after data collection. Because further physical access to the other two guitar amplifiers was not possible, the Deluxe was used as a baseline to find and overlay speaker cone centers of the other two amplifiers to ensure that similar areas were compared between amplifier models. The layouts of the amplifier dimensions within the measurement grid are shown in Figure 3.3-1 below.

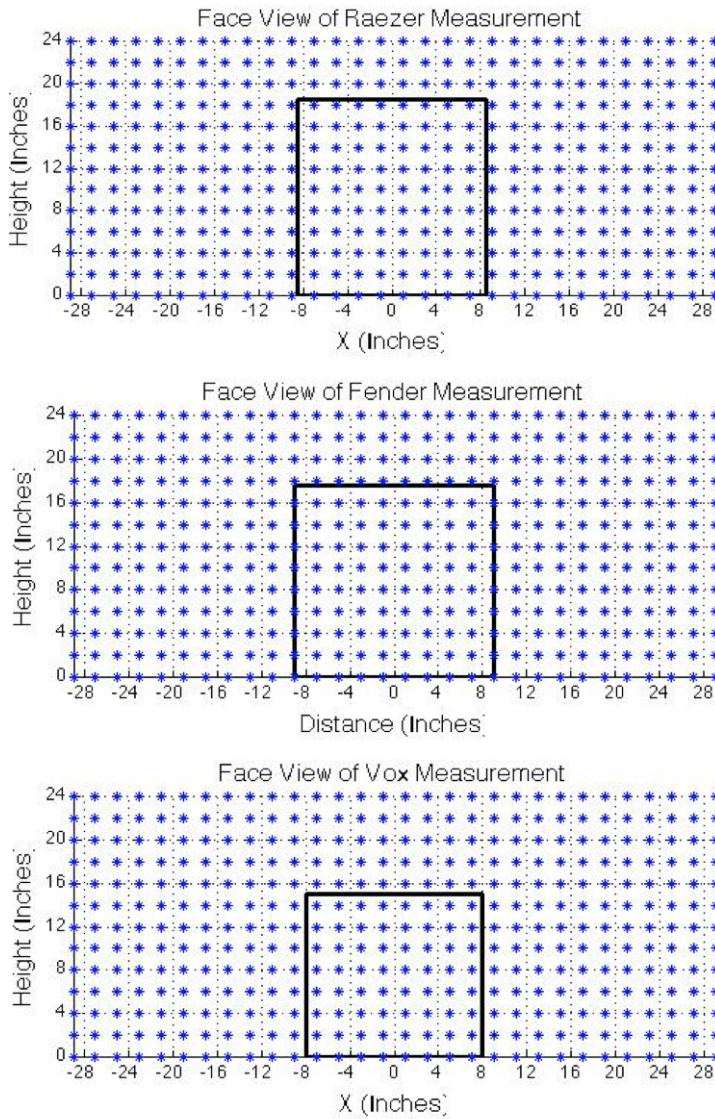


Figure 3.3-1 The dimensions of the amplifiers outlined in black overlaid with the grid of microphone array capsules in the face plane measurement grid (Matthew, 2012)

A custom Sennheiser microphone array was placed at the face-plane of each amplifier at a distance of two inches to measure the impulse response at each capsule location. The microphone array had capsules every two inches. The capsule corresponding to the center of the Deluxe's speaker was selected, and three capsules to the right and left as well as three capsules up and down from this center capsule were included to serve as the center of the amplifier.

This method resulted in a 7x7 matrix of impulse responses representing the sound around the speaker cone. This 7x7 matrix was stored as a cell array wherein each cell contained the impulse response captured by the corresponding microphone capsule. These impulse responses were then transformed to the frequency domain using the Discrete Fourier Transform (DFT) to obtain the magnitude in dB of the frequency responses. The frequency responses in dB were stored in cell arrays for each capsule position for each amplifier.

The Deluxe's 7x7 impulse response array served as a reference area against which to compare the other two amplifiers. To identify and isolate the respective 'center' of the other two amplifiers, the entire 13x28 grid for each amplifier was first analyzed. A Matlab function was created to loop through 7x7 grids starting at the top left of the array. This grid was moved column-wise and row-wise respectively through the array, and the differences between the magnitudes of the frequency responses at each capsule position were stored. Once all positions had been covered, the 7x7 grid where the absolute value of the standard deviation in the stored differences was lowest was used as the 'center' of each amplifier. An overview of the alignment method is shown in Figure 3.3-2.

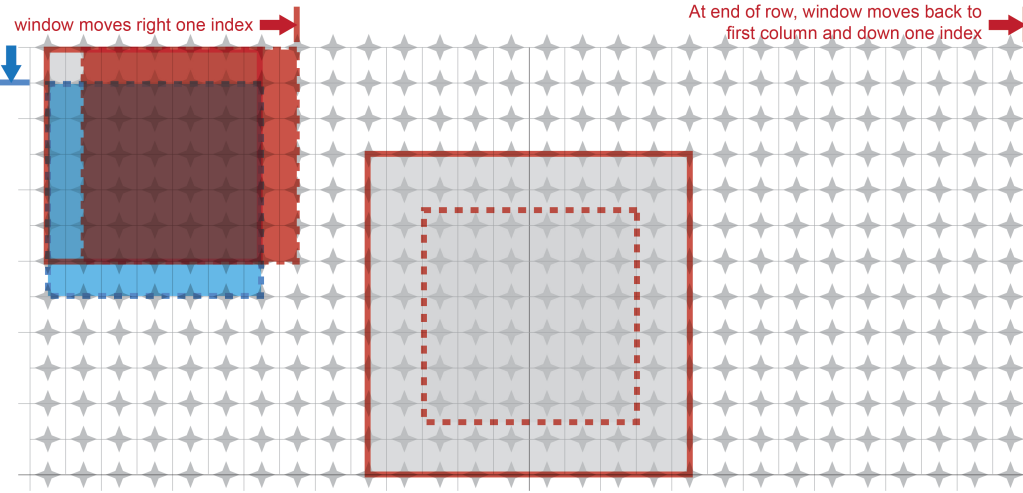


Figure 3.3-2 Outline of how the amplifier centers were determined. The dotted line in the grey square represents the centered area of the Fender Deluxe. The moving window moves across the grid (the red square) through all column indices and then down one row (the blue square), and repeats through all positions. The results are stored, and the 7x7 grids on each of the other two amplifiers where the absolute value of the standard deviation was lowest were used as the centers of the amplifiers.

### 3.4. Pre-processing: convolution and deconvolution

Throughout the rest of this thesis, “correct” means a signal that was originally convolved with a given amplifier was also deconvolved from that same amplifier; “incorrect” means a signal that was originally convolved with one amplifier but was then deconvolved from another.

#### 3.4.1. Convolution

Convolution is a technique widely used in signal processing. In a linear time-invariant system, the output of the system can be completely described as a function of the input signal and the impulse response of the system. An input signal is combined mathematically

with the impulse response of the system, and the resulting output represents the effect of the system on the input signal. The equation below shows the convolution equation in the time domain:

$$y[n] = \sum_{k=-\infty}^{\infty} h[k]x[n-k]$$

Recording the guitars through the different amplifiers would have introduced inconsistencies to the recorded output due to differences and small variations in the recording environments. To ensure consistency of testing sounds played through the centered amplifier matrices and avoid differences introduced through actually recording the guitar samples through the amplifiers, convolution was used to test recorded guitar signals through each amplifier because convolution can “make a signal take on the characteristics of [a] system” (Roads, 1996). This means that the output would not suffer from inconsistencies between the data sets introduced through recording.

Convolution can be performed in the time domain, but this method is computationally expensive and notoriously time consuming. However, as the Law of Convolution states, convolution in the time domain is equivalent to multiplication in the frequency domain. In order to perform the much more computationally efficient frequency domain multiplications, DFTs were performed on the signals and the amplifier impulse responses in order to obtain frequency domain representations. Multiplication was performed in the frequency domain, and the inverse DFT was performed to transform the resulting convolved signals back into the time domain.

A guitar sample was selected randomly from the 1x10 array of training guitar samples described in section 3.3. The sample was then convolved with the impulse response at each capsule position across the 7x7 impulse response array of capsules around the ‘center’ of the speaker cone for each amplifier. This process was repeated fifty times for each amplifier. The results of the convolutions from each amplifier were stored in three separate, labeled, 1x50 cell arrays referred to henceforth as the ‘convolution arrays’.

### *3.4.2. Deconvolution*

The next step was to perform deconvolution on each of the convolutions in order to try to isolate correct deconvolution versus incorrect ones.

As the name implies, deconvolution is the process of separating an input signal from the effects of an LTI system. Deconvolution is not a perfect reconstruction of the original signal due to the time smearing artifacts from convolution, but a reasonable reconstruction of the input signal can be obtained (Roads, 1996). Equation 3.4.2-1 shows how a convolved signal can be deconvolved in the frequency domain:

$$y = x * h = X \cdot H = Y$$

$$\hat{x} = \frac{Y}{H}$$

Deconvolution can also be performed in the frequency domain, which offers the same computational savings as frequency domain, or, ‘fast’ convolution. Frequency domain deconvolution is the inverse process of fast convolution. The DFT of a convolved signal is divided by the DFT of the impulse response of the system (Press, Teukolsky, Vetterling, Flannery, 1992). While methods exist to decrease the amount of noise present in the

deconvolved signal, this study did not employ such noise reduction techniques because the resulting noise is actually what enabled amplifier identification.

Deconvolving a signal from the system with which it was originally convolved will result in some artifacts due to time smearing that occur during the convolution (Roads, 1996)(Stockham, 1971)(Stockham, 1975). Even a correctly deconvolved signal results in some degree of noise. If a convolved signal is deconvolved from a system with which it was not originally convolved, it follows that there should be residual artifacts, distortion, and noise that were not part of the original signal.

A large ‘training’ dataset that contains many correct and incorrect deconvolutions would be analyzed to determine a method of identifying the correct amplifier. The resulting noise and artifacts should be distinguishable from those resulting from a correct deconvolution. A method to identify a clean guitar signal versus one that has been deconvolved from the incorrect amplifier should emerge through an analysis of the resulting correct and incorrect signals after deconvolution. Using a method of elimination, a best guess can be made as to which amplifier was used to make a recording.

The dataset of deconvolutions was created with an identical process for each amplifier. To create the deconvolution array, a 3x50 cell array was pre-allocated in memory for each of the amplifiers. Because this step required such large amounts of processing time, memory, and disk space, each set of deconvolutions was calculated separately over multi-hour periods of allowing the functions to run.

The 1x50 convolution array was loaded along with all three 7x7 impulse response arrays. The convolved signal at each index of the convolution array was deconvolved from each impulse response. The results of the deconvolutions were stored in the

corresponding row/column of the newly created deconvolution array. A diagram outlining this process is shown below in Figure 3.4-1.

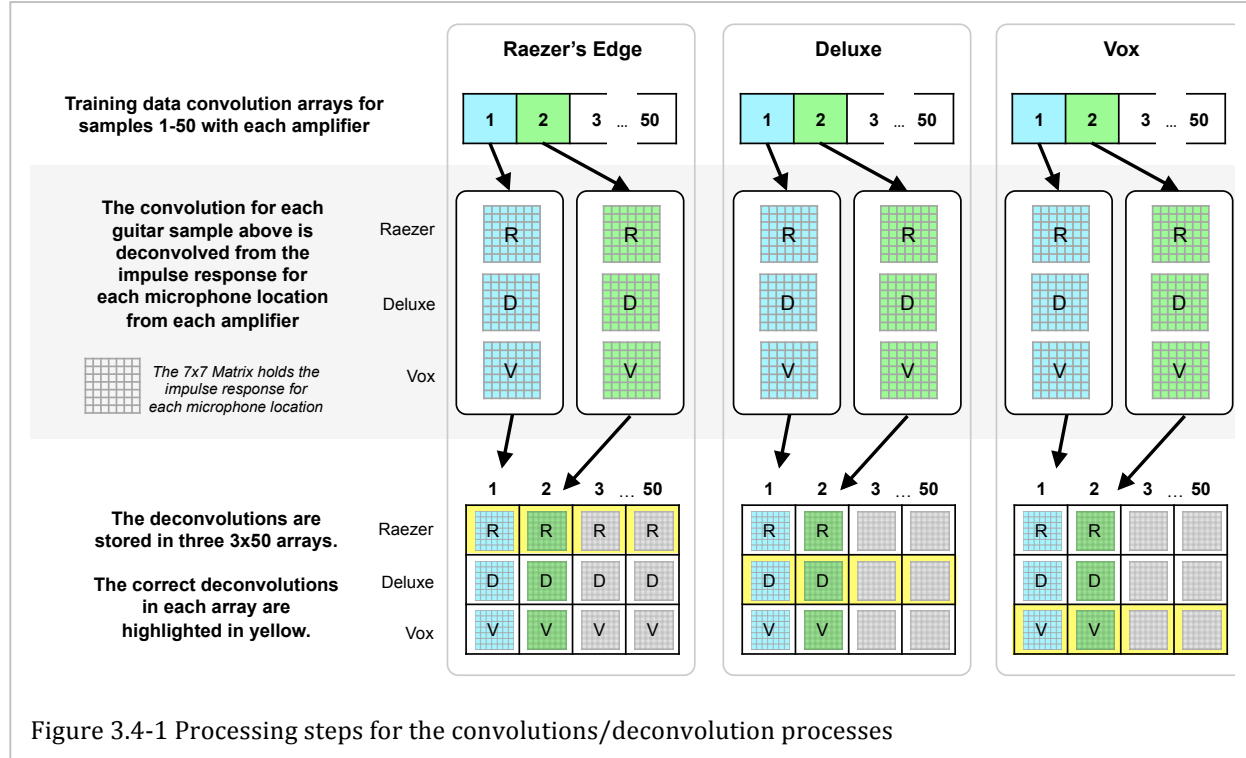


Figure 3.4-1 Processing steps for the convolutions/deconvolution processes

The three deconvolution arrays were identical to each other in structure. In each array, row values represented the deconvolutions from each amplifier. Row number one contained Raezer's Edge deconvolutions; row number two contained Fender Deluxe deconvolutions; row number three contained Vox deconvolutions. This standard order of Raezer's Edge, Fender Deluxe, and Vox was maintained throughout every step in this thesis to maintain consistency. The column values of this array contained the same fifty guitar signals in the same order as in the convolution array.

These deconvolution arrays comprised the final set of three, 3x50 cell arrays with a total of 450 deconvolutions (approximately 65 GB of data). Within the Raezer's Edge deconvolution array, each cell in row number one contained a correct deconvolution

because it was deconvolved with itself. Rows two and three contained incorrect deconvolutions. The structure of the deconvolution data was the same for the other two amplifiers' deconvolution arrays, except that in the Deluxe array, row two contained the correct deconvolutions, and in the Vox array, row three contained the correct deconvolutions.

### **3.5. Post-processing analysis**

Analysis of the training data set identified what kinds of artifacts and noise resulted from the incorrect deconvolutions. The training data was processed and the results were then used to inform further testing with the two sets of test guitar signals. The following section describes how the training data was processed and analyzed. Following the training data processing, the test guitar data sets were subjected to the same treatment. Following the data preparation, identification was performed using two different methods.

#### *3.5.1. Listening test performed on training data*

Prior to any programmatic approach to analysis, an informal listening test was performed to provide a simple confirmation that the author's intuition about the presence of noise or artifacts after incorrect deconvolution would hold true. In this listening test, a few examples of correct and incorrect deconvolutions were written to .WAV files. While the correct deconvolutions resulted in a clean sound without any noticeable noise or artifacts, the incorrect deconvolutions resulted in various amounts of high and low frequency noise in the form of high pitched ringing, feedback, and a comb-filtering sound.

### *3.5.2. Octave band filtering on training data*

This listening test result indicated that the first step of the formal, programmatic analysis would be to apply an octave band filter to emphasize these artifacts. Octave band filtering was also performed in Roginska, Case, Madden, and Anderson (2012), Madden (2012), Roginska, Matthew, Madden, Anderson, and Case (2012), Matthew (2012) and Matthew and Blackmore (2013). The octave band filtering in these studies allows for data reduction, and a similar filtering was utilized for this analysis.

The deconvolution data of each of the three amplifiers was passed through three separate, different types of octave band filters in order to create a robust analysis of the deconvolution data and enable noise pattern identification. The octave bands selected for filtering were 1/12<sup>th</sup>-octave, 1/6<sup>th</sup>-octave, and 1/3<sup>rd</sup>-octave. These three filter sizes were chosen because they offered varying degrees of granularity in the analysis without overly increasing the amount of processing time. Each of the filters started with the musical pitch A<sub>2</sub> and covered six octaves through which data was filtered. The number of frequencies in each filter is listed in Table 3.5-1 below:

Octave Band Filter	Number of frequencies
1/12 <sup>th</sup>	72
1/6 <sup>th</sup>	36
1/3 <sup>rd</sup>	24

Table 3.5-1 Number of frequencies in each octave band filter

### *3.5.3. Octave band filter results storage*

The octave band filter results were then stored in Octave Band Filtered Deconvolution (OBFD) Arrays in three amplifier sets. These nine OBFD Arrays are comprised of: Three

1/12<sup>th</sup> OBFD Arrays (one for each amplifier); three 1/6<sup>th</sup> OBFD Arrays (one for each amplifier); and three 1/3<sup>rd</sup> OBFD Arrays (one for each amplifier). Each OBFD Array was 3x50, and contained the deconvolution results of each amplifier at the respective octave band. A diagram showing how the data was organized for each OBFD Array is depicted below in Figure 3.5-1.

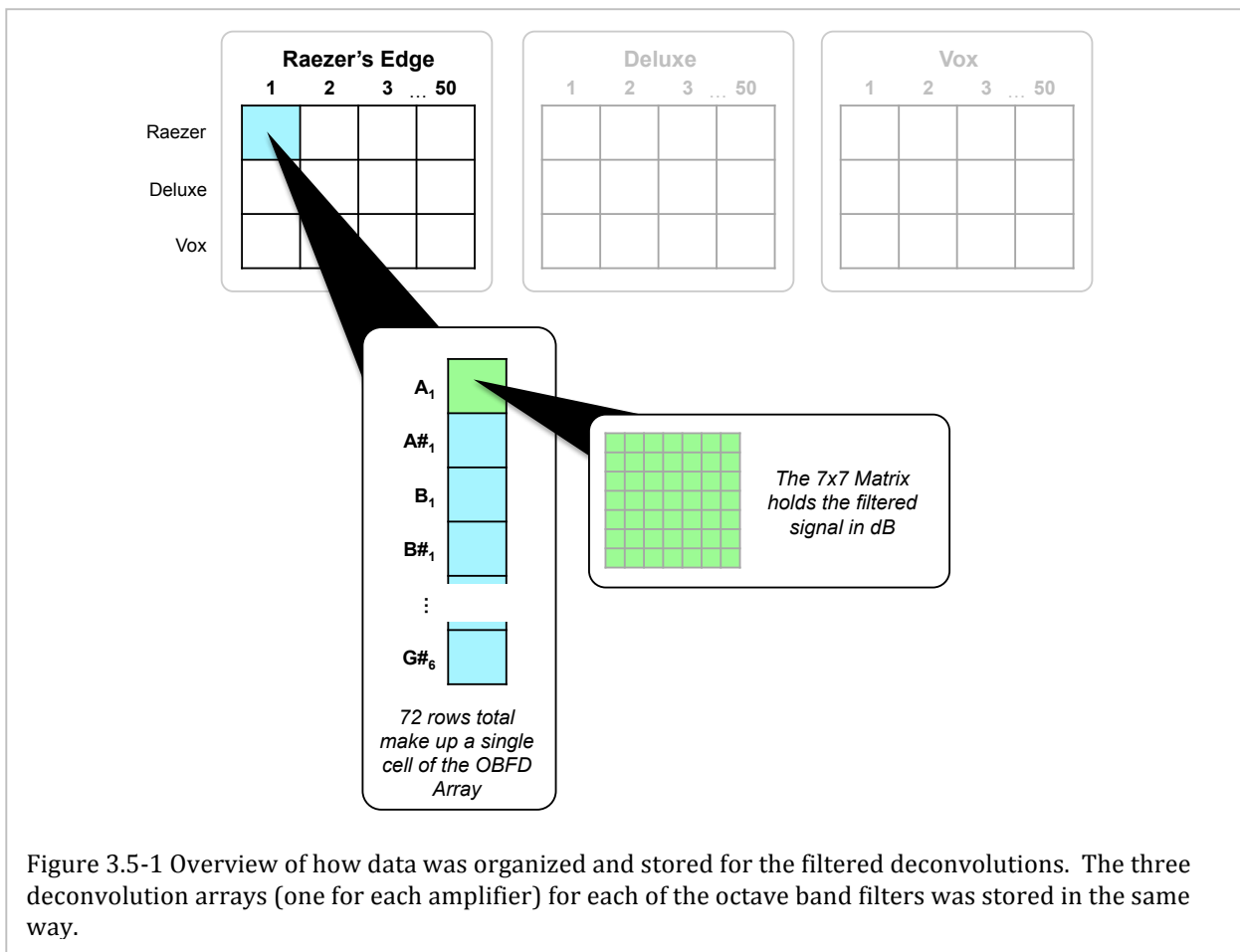


Figure 3.5-1 Overview of how data was organized and stored for the filtered deconvolutions. The three deconvolution arrays (one for each amplifier) for each of the octave band filters was stored in the same way.

Each cell in an OBFD Array contained an array of filter results that varied in size according to number of divisions in the respective octave bands as represented in Table 3.5-2 below:

Octave Band Filter	Array Size
1/12 <sup>th</sup>	72x1
1/6 <sup>th</sup>	36x1
1/3 <sup>rd</sup>	24x1

Table 3.5-2 Filter result arrays within one cell of an OBFD Array

The cell array at each center frequency contained a 7x7 matrix of scalar dB values. These dB values represented the magnitude of each microphone capsule around the center of the guitar amplifier at a given center frequency.

Plots of a few of the guitar samples depicting correct deconvolutions versus incorrect deconvolutions at different frequencies will be presented in the Results section. A diagram showing how the data was organized for each OBFD Array cell is depicted in Figure 3.5-1.

#### *3.5.4. Principal component analysis (PCA) data preparation*

PCA was then performed on the data resulting from the octave band filtering to reveal any data clusters that arose from the filtered deconvolutions by reducing the number of data dimensions. This process highlights the dimensions that contain the greatest variance and reorganizes the data accordingly. The desired result of PCA would show clustering of the data by the most important components present (Schiens, 2009).

The data was first restructured into a single large ‘PCA Staging Matrix’ for each filtered data set to enable PCA. This restructuring resulted in three PCA Staging Matrices. Each PCA Staging Matrix contained three amplifier OBFD Arrays. The three PCA Staging Matrices correspond with the type of Octave Band Filter used, and they were structured according to Table 3.5-3 below:

Octave Band Filter	Matrix Size	Number of pitches
1/12 <sup>th</sup>	32,400x49	72
1/6 <sup>th</sup>	16,200x49	36
1/3 <sup>rd</sup>	10,800x49	24

Table 3.5-3 PCA Staging Matrix sizes. The difference in matrix size reflects the varying dimensions of the OBFD Arrays.

To create each PCA Staging Matrix, a function was created in Matlab that looped through each OBFD Array to reorganize its internal data. The 7x7 matrices at the most granular depth of an OBFD Array were reshaped into 1x49 vectors. The 49 columns in each vector comprise the 49 columns in each PCA Staging Matrix.

The rows for each PCA Staging Matrix represented filtered deconvolution samples grouped by amplifier. The OBFD arrays were processed in a manner that all filtered samples from each amplifier were grouped together. For example, for the 1/12<sup>th</sup> PCA Staging Matrix, the first 10,800 rows (of 32,400 total rows) contain the Raezer's Edge filtered samples; the next 10,800 rows contained the Deluxe filtered samples; and the final 10,800 rows contained the Vox filtered samples.

### 3.5.5. *PCA processing*

The PCA Staging Matrices were processed through Matlab's built-in *princomp* function. The first three principal components were selected from the *princomp* output matrices containing PCA scores. The results were plotted on three dimensional scatter plots where each axis represented a principal component. Only the first three components were selected as a starting point for analysis. A consistently linear, easily observable clustering emerged from the plotting of the first three components. This consistent clustering justified the importance of the first three components and indicated that the remaining

components were redundant and it was unnecessary to analyze them further. These plots will be explained in more detail in the Results (Section 4) below.

### 3.6. Identification

The final step in the processing sequence was to attempt identification of the guitar amplifier for twenty test data samples. The guitar samples used for testing were selected randomly from the guitar data set, and each sample was convolved with one randomly selected guitar amplifier. This process ensured that the convolution process was done blindly.

Two methods for identification were explored. The first method relied on comparisons to the training data set to attempt amplifier identification. The second method attempted amplifier identifications for each test sample using only the data from the processing methods described above applied to itself.

#### 3.6.1. *Method One: comparison of test data against training data*

Using the data points on the hyperplane created through PCA, test signals were passed from the test data sent through all of the same processing steps described above for the training data set. The result was projected into the same three-dimensional space as the training data.

The best-fit line for the training data correct deconvolutions was calculated using a Matlab function called *best\_fit\_line* (Stafford, 2005). This function takes the three-dimensional points calculated from the three principal components, and it returns values that allow for the calculation of “the best line in the minimum mean square orthogonal

distance sense" (Stafford, 2005). See Appendix 8.2 for the actual function and how the line was calculated from the *best\_fit\_line.m* function.

A new Matlab function was created to calculate the orthogonal distance from each data point to the best-fit line of the training data. This function is shown in Appendix 8.2. The average orthogonal distance from the best-fit line of the training data was then calculated for each amplifier. The amplifier with the lowest average orthogonal distance from the best-fit line received was selected as the correct one. This determination is expressed through a level of confidence that the associated amplifier is the source. For the training data comparison, the amplifier with the smallest average orthogonal distance from the best-fit line received the highest confidence level (measured as a percentage). To calculate the confidence level, the following formula was used:

$$100 \left( 1 - \frac{\text{average distance}}{\sum \text{distance}} \right) = \% \text{ confident}$$

### *3.6.2. Method Two: comparison of test data against itself*

A second method of amplifier identification was explored. This method was derived after an analysis of Method One's results and compares the test data to its own linearity rather than to the linearity of the training data. The smaller data set using the Fender Telecaster was also tested, only using this method to ascertain if these techniques could be extended to other guitars.

This thesis will refer to linearity as the tendency for data points to fall in a predominately straight line when projected in to three dimensions and observed. This term

is not to be confused with 'linearity' defined in digital signal processing literature as satisfying the properties of superposition and scaling.

A best-fit line was measured for each of the deconvolved and filtered test results for each amplifier, using the same function described in Method One. The three lines were then projected into the three dimensional space, and the amplifier with the lowest standard deviation of the orthogonal distance from the best-fit line received the highest confidence level (measured as a percentage). The measure of orthogonal distance in this method was performed in exactly the same way as in Method One. However, after analyzing the inaccuracy in Method One, it was decided to use the standard deviation from the best-fit line rather than the average orthogonal distance. To calculate the confidence level, the following formula was used:

$$100 \left( 1 - \frac{\text{average distance}}{\sum \text{distance}} \right) = \% \text{ confident}$$

### *3.6.3. Measuring precision*

The two identification methods were tested for precision by measuring how often the system correctly determined the guitar amplifier with which the test signal had been convolved. The precision was represented as a percentage and was enabled by storing the input and output parameters.

During each identification test (described in sections 3.6.1 and 3.6.2), the input signals and output convolutions associated with the blinded signal were stored separately as known parameters. To determine the correct known amplifier, the deconvolution process

was repeated with the convolved signal on each amplifier. The deconvolved signals were then compared to the original input signals by taking the absolute value of the differences between the input signals and the deconvolved signals. The result with the smallest difference was the known correct amplifier.

The percentage of times where this known result matched the identification test result determined the precision of the identification system. A high percentage indicated high precision (or many times identifying the correct amplifier), and a low percentage indicated low precision (or few times identifying the correct amplifier).

## 4. Results

Prior to running the tests in Method One described in section 3.6.1, it was not anticipated that a second approach would be needed. After examining the results of amplifier identification using Method One, it was decided to try a second approach. The second approach produced much better results. The results from both methods will be presented in this section.

### 4.1. Deconvolution results

Many differences are easily observed between the correct and incorrect deconvolutions. These differences are audible as well as observable in spectral plots of the face plane output after deconvolution. A function was created to analyze the deconvolution arrays at different octaves of an input note. Several examples of these differences can be seen in Figures 4.1-1, 4.1-2, and 4.1-3 below. These figures display information for only a single note in the scale (F). The plots in Figures 4.1-1 – 4.1-3 show spectral plots for the 7x7 grid at the face-planes of the amplifiers.

Consistent throughout the plots is shown the noisiness of the incorrect deconvolutions and the relatively stable plots of the correct deconvolutions.

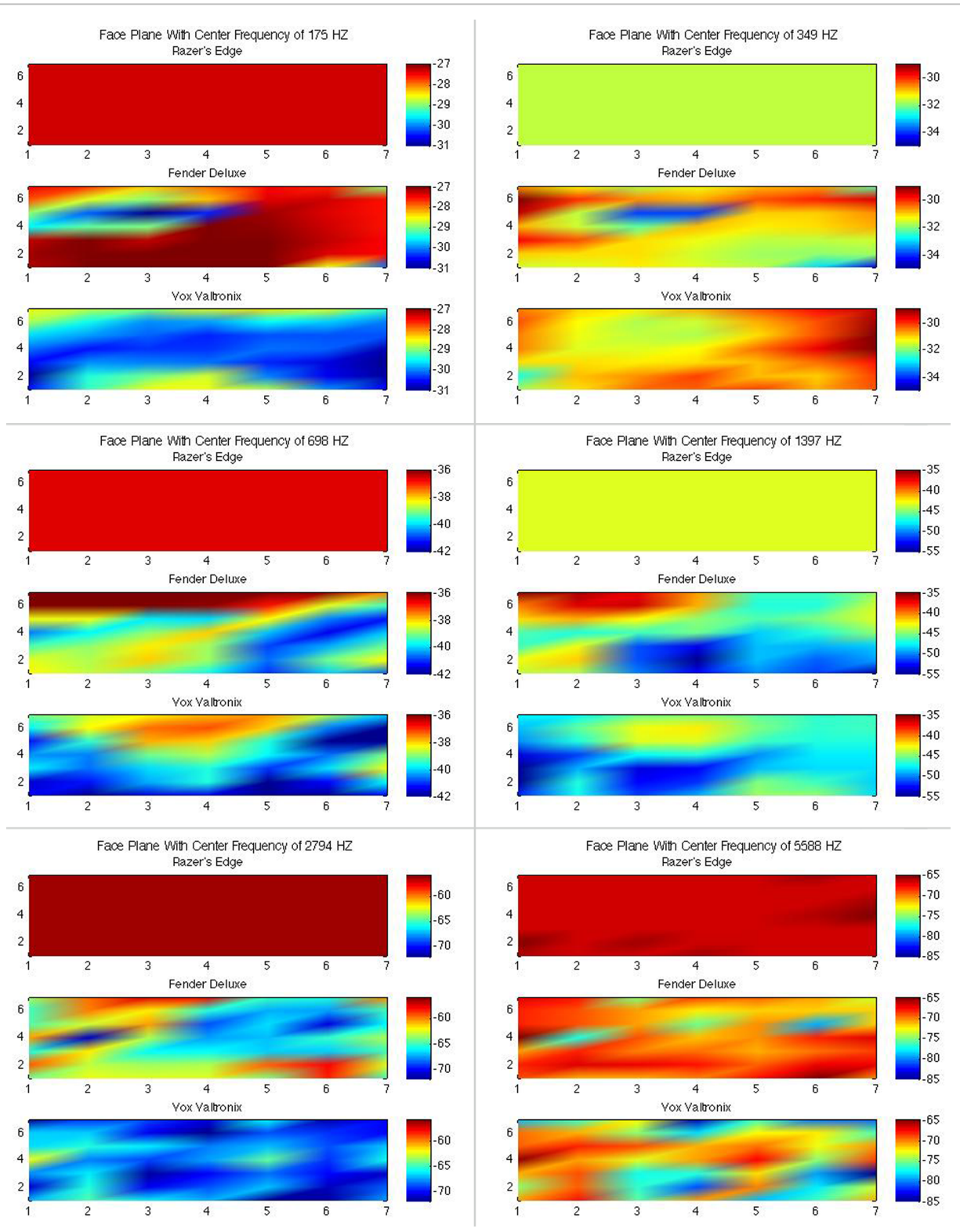


Figure 4.1-1 Deconvolutions from the Raezer's Edge deconvolution array across 6 octaves of F. The Raezer's Edge was the correct deconvolution here, and the other two amplifiers were incorrect. The Raezer's Edge is the top amplifier in each of the six plots.

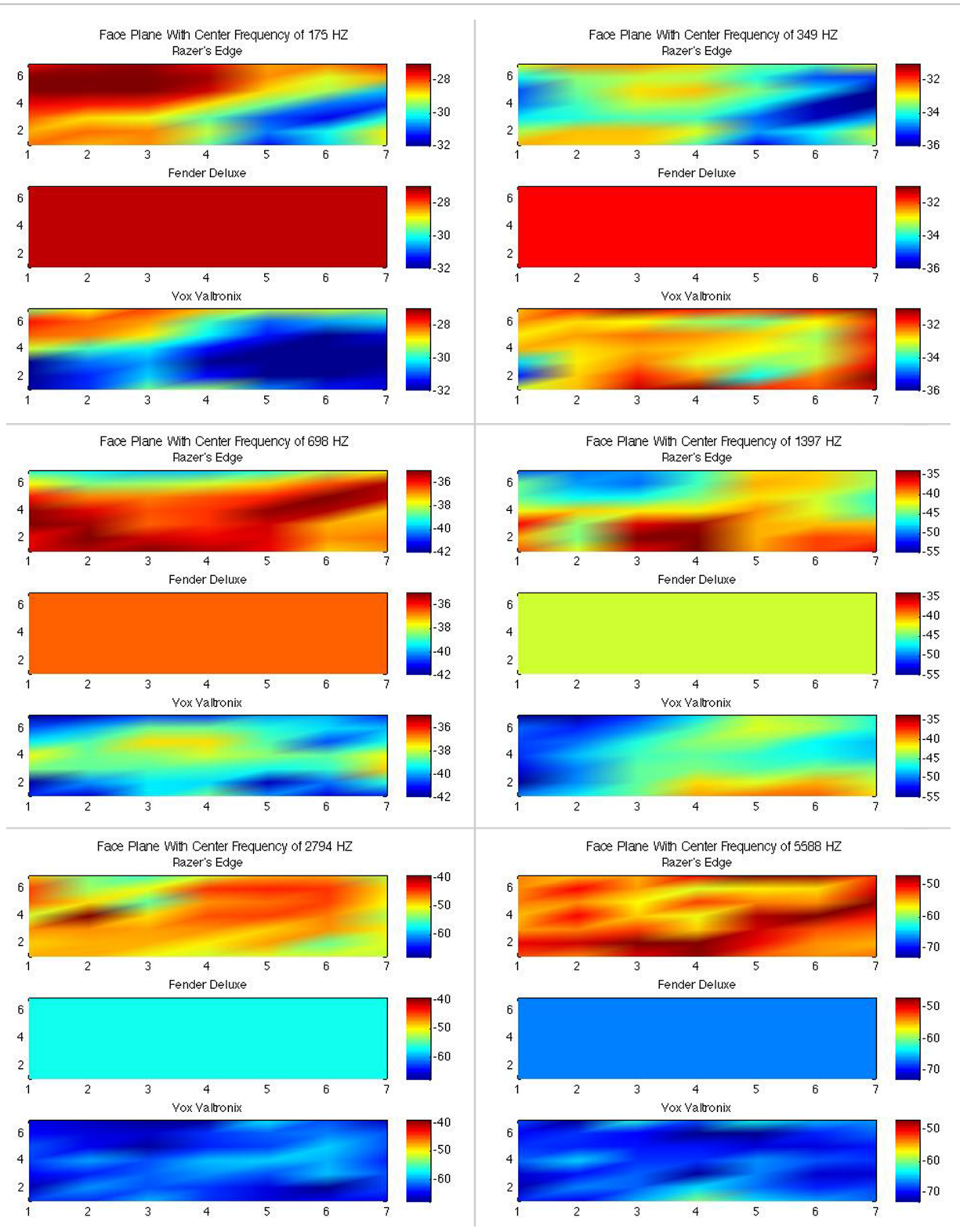


Figure 4.1-2 Deconvolutions from the Fender Deluxe deconvolution array across 6 octaves of F. In this example, the Deluxe was the correct deconvolution, and the other two amplifiers were incorrect. The Deluxe is the middle amplifier in each of the six plots.

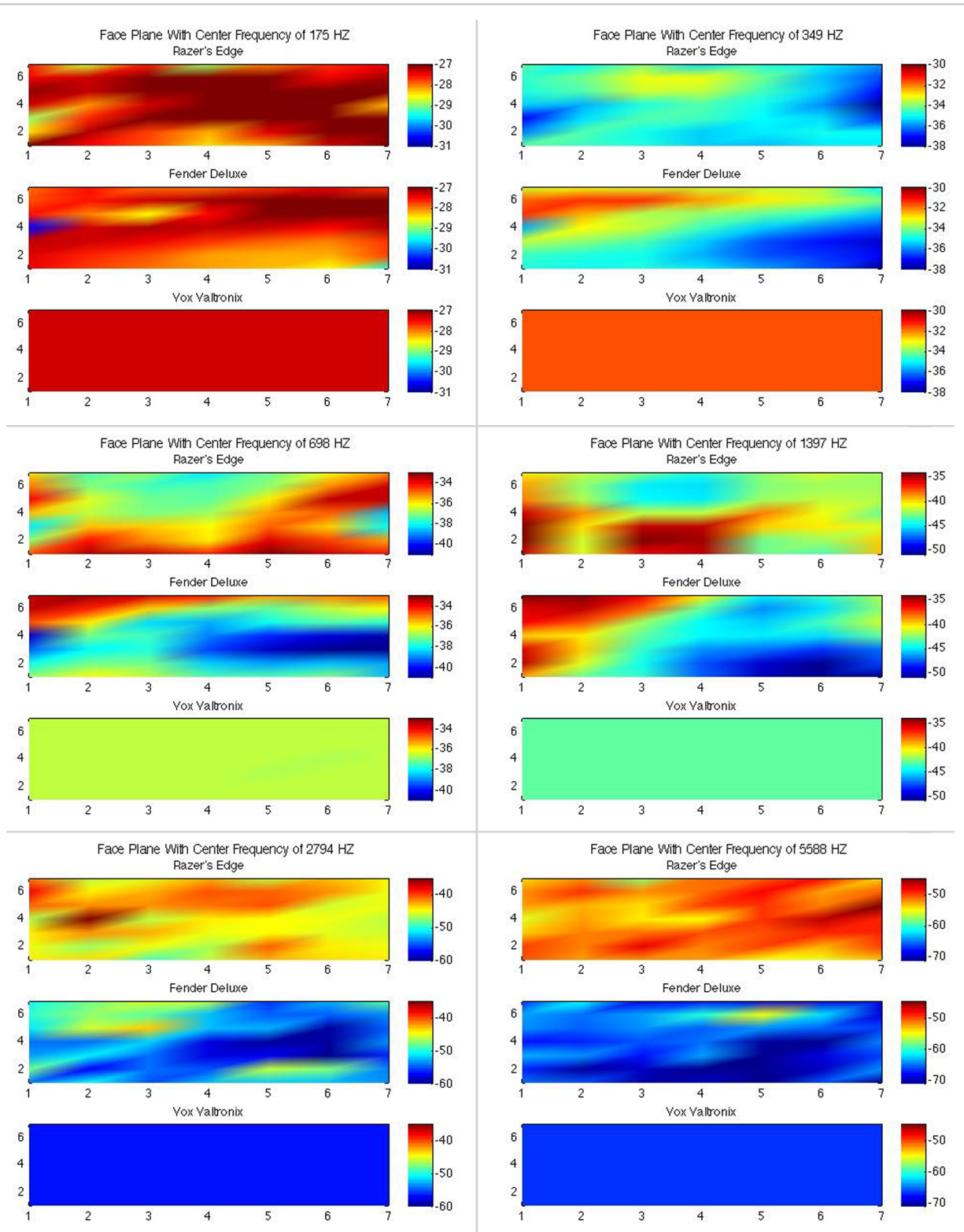


Figure 4.1-3 Deconvolutions from the Vox Valvetronix deconvolution array across 6 octaves of F. In this example, the Vox was the correct deconvolution, and the other two amplifiers were incorrect. The Vox is the bottom amplifier in each of the six plots.

In Figure 4.1-1 the Raezer's Edge (the top amplifier in each of the plots in 4.1-1) was the known correct amplifier for the deconvolutions. These plots show that the Raezer's Edge radiation pattern remains stable across all octaves for this frequency. This plot is consistent with how the .WAV outputs sounded during the informal listening test. Since the Raezer's Edge was the correct amplifier in Figure 4.1-1, less noise would be expected and is shown in the Raezer's Edge output when compared to the other two amplifiers.

The other two amplifiers display patterns of wildly differing outputs at every octave, and they differ sharply between each capsule across the face plane. The radiation patterns change quite drastically from octave to octave while the radiation patterns shown in the Raezer's Edge plots do not exhibit much change across the capsules in the face plane.

In Figure 4.1-2, the Fender Deluxe was the known correct amplifier for the deconvolutions. In this set of plots, a pattern similar to the pattern in Figure 4.1-1 can be seen; there are consistent radiation patterns across the six octaves at each capsule position for the Deluxe. The Raezer's Edge and the Vox display the same variability across octaves and at each microphone capsule position.

The Vox amplifier was the known correct amplifier for deconvolution in the plots shown in Figure 4.1-3. Interestingly, this set of plots shows that the overall spatial variability remains relatively consistent across octaves for the Vox, but the output magnitudes change quite a bit across octaves. This may be due to the Vox's smaller 8-inch speaker (the other two amplifiers have 12-inch speakers).

Figures 4.1-1, 4.1-2, and 4.1-3 display plots of the filtered deconvolution arrays of six octaves for only the single musical pitch of F. Examples of octave band filtered plots for different pitches (A and C) are presented in the appendix as Figures 8.1-1 through 8.1-6.

These notes plotted comprise the major triad F major (F, A, and C). These plots reinforce the observations presented above because of the noisiness of the incorrect deconvolutions and the stable radiation patterns of the correct deconvolutions remains consistent across all notes. All of the differences as well as the presence of observable consistencies from the octave band filtered deconvolutions point to measurable patterns within the deconvolution data.

#### **4.2. Training data results (Method One)**

The result of running PCA on all of the data points revealed a strong clustering between the correct deconvolutions. Figure 4.2-1 below shows a three-dimensional plot of the first three principal components for the 1/12<sup>th</sup>-octave filtered deconvolutions for all data points, and Figure 4.2-2 below shows only the correct 1/12<sup>th</sup>-octave filtered deconvolutions with the line of best fit overlaid.

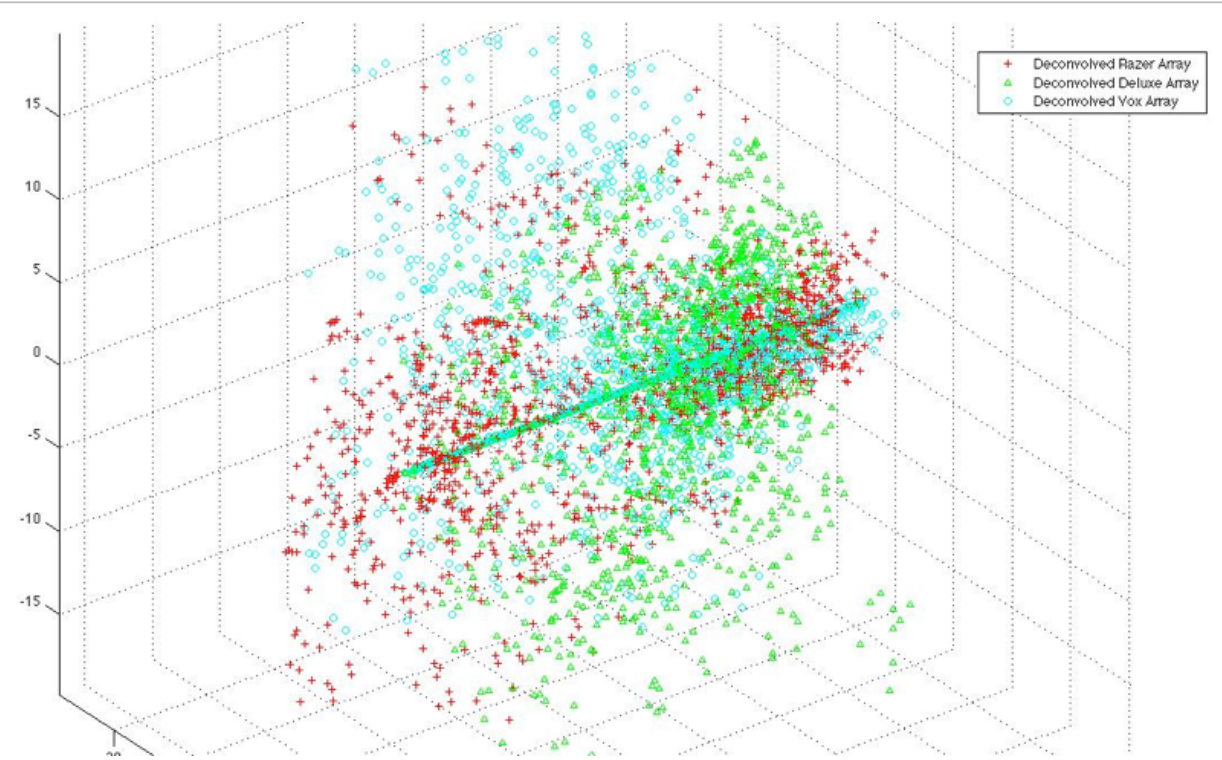


Figure 4.2-1 Plot of first three principal components obtained from PCA filtered with 1/12th octave bands

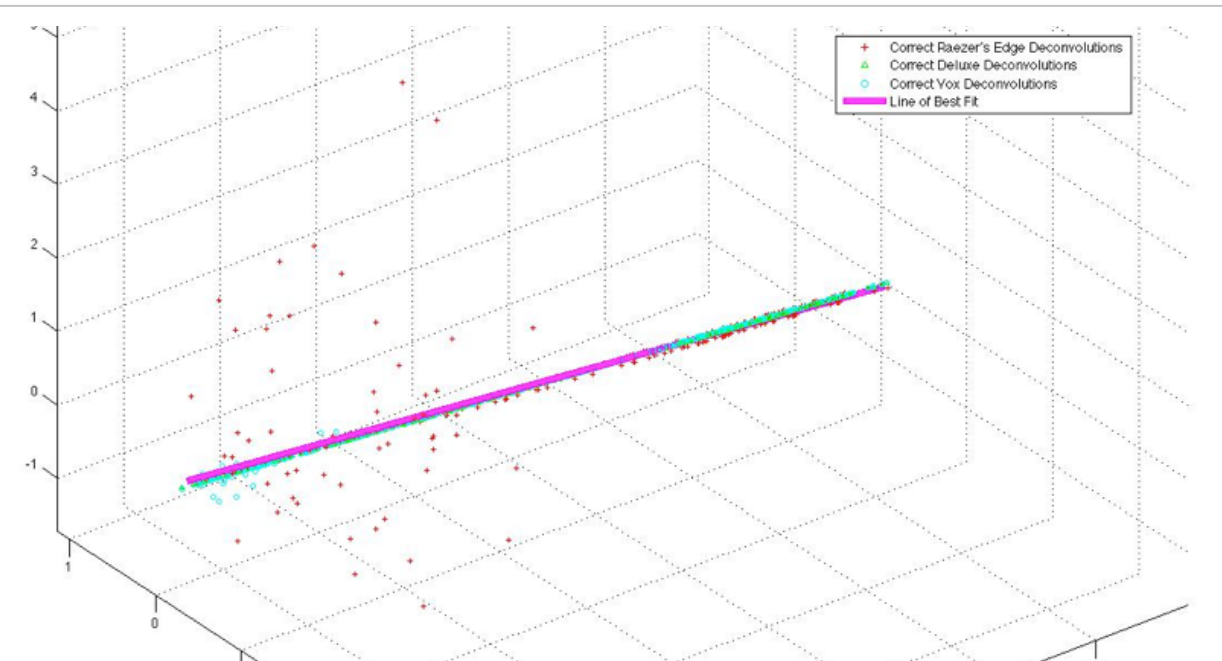
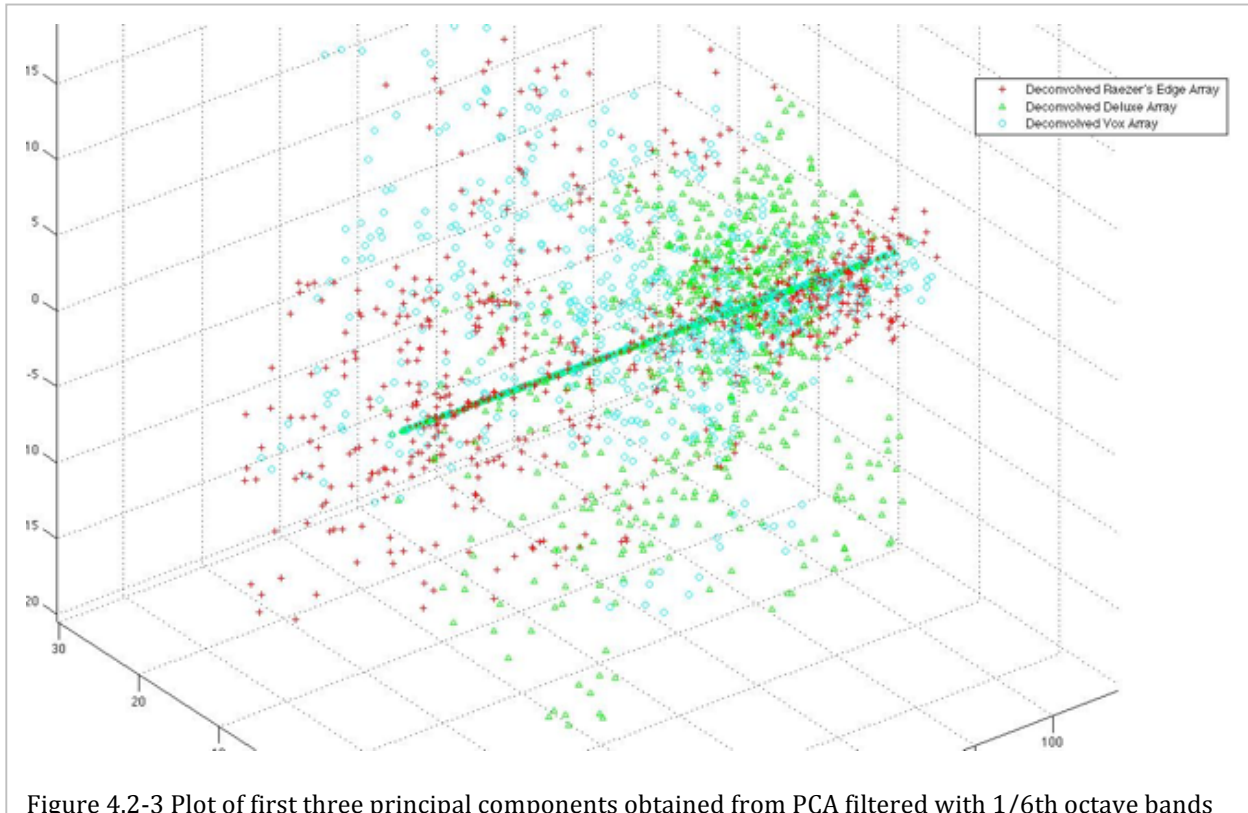


Figure 4.2-2 First three principal components, correct deconvolutions only, filtered through 1/12th octave bands, with line of best fit overlaid

The most interesting feature observed from these plots is the tendency for correct deconvolutions to fall in a relatively straight line while the incorrect deconvolutions are widely scattered. Both the training data set and the test data set displayed these tendencies.

Even with many fewer data points from 1/6<sup>th</sup> and 1/3<sup>rd</sup> octave band filters, the linearity of the correct deconvolutions vs. the widely scattered points from the incorrect deconvolutions remains consistent. Figures 4.2-1 and 4.2-2 are the same as Figures 4.2-3 and 4.2-4 except that they show 1/6<sup>th</sup> octave filtered deconvolutions, and Figures 4.2-5 and 4.2-6 display this information for 1/3<sup>rd</sup> octave-filtered deconvolutions.



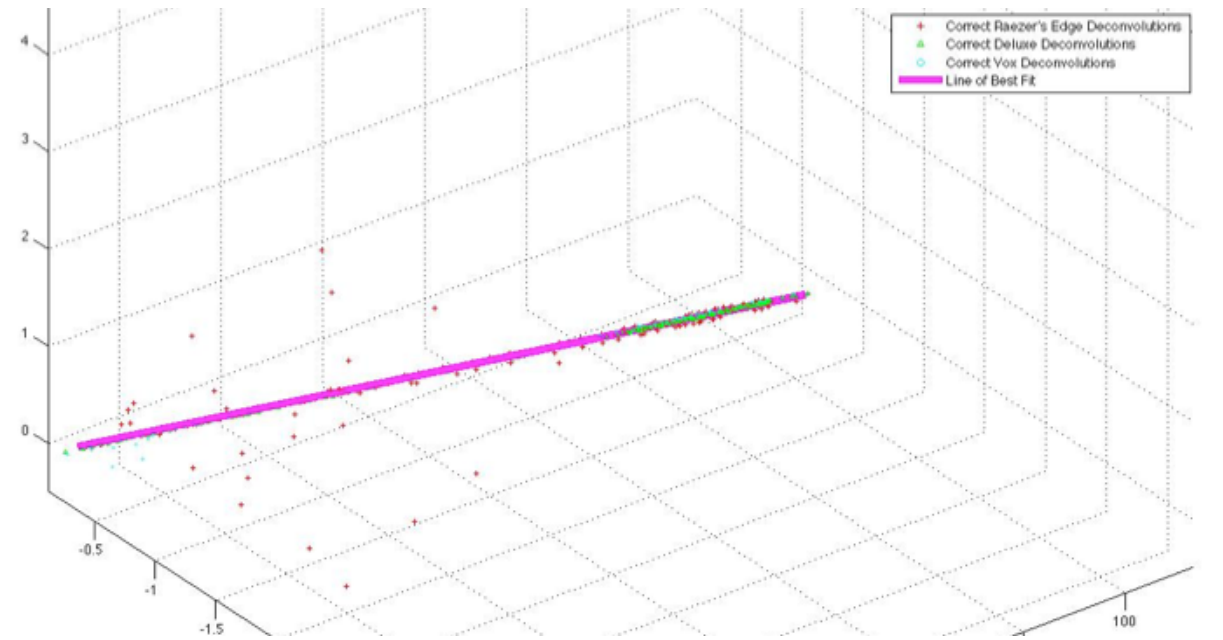


Figure 4.2-4 First three principal components, correct deconvolutions only, filtered through 1/6th octave bands, with line of best fit overlaid

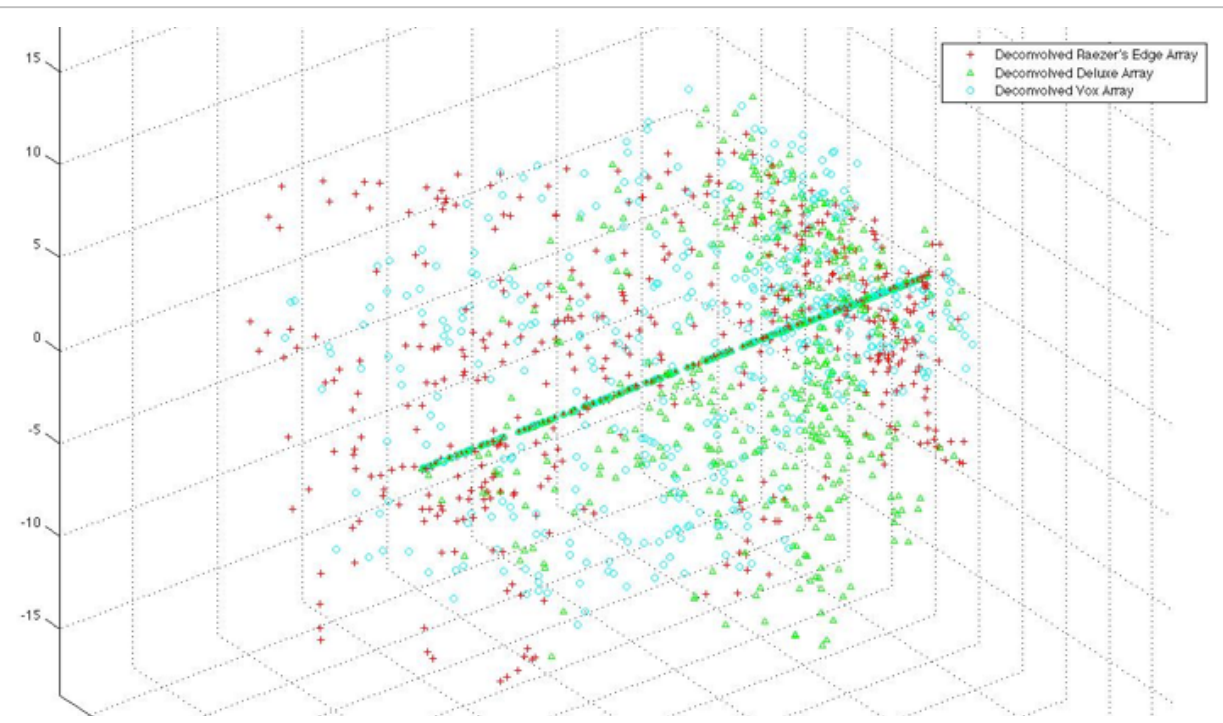
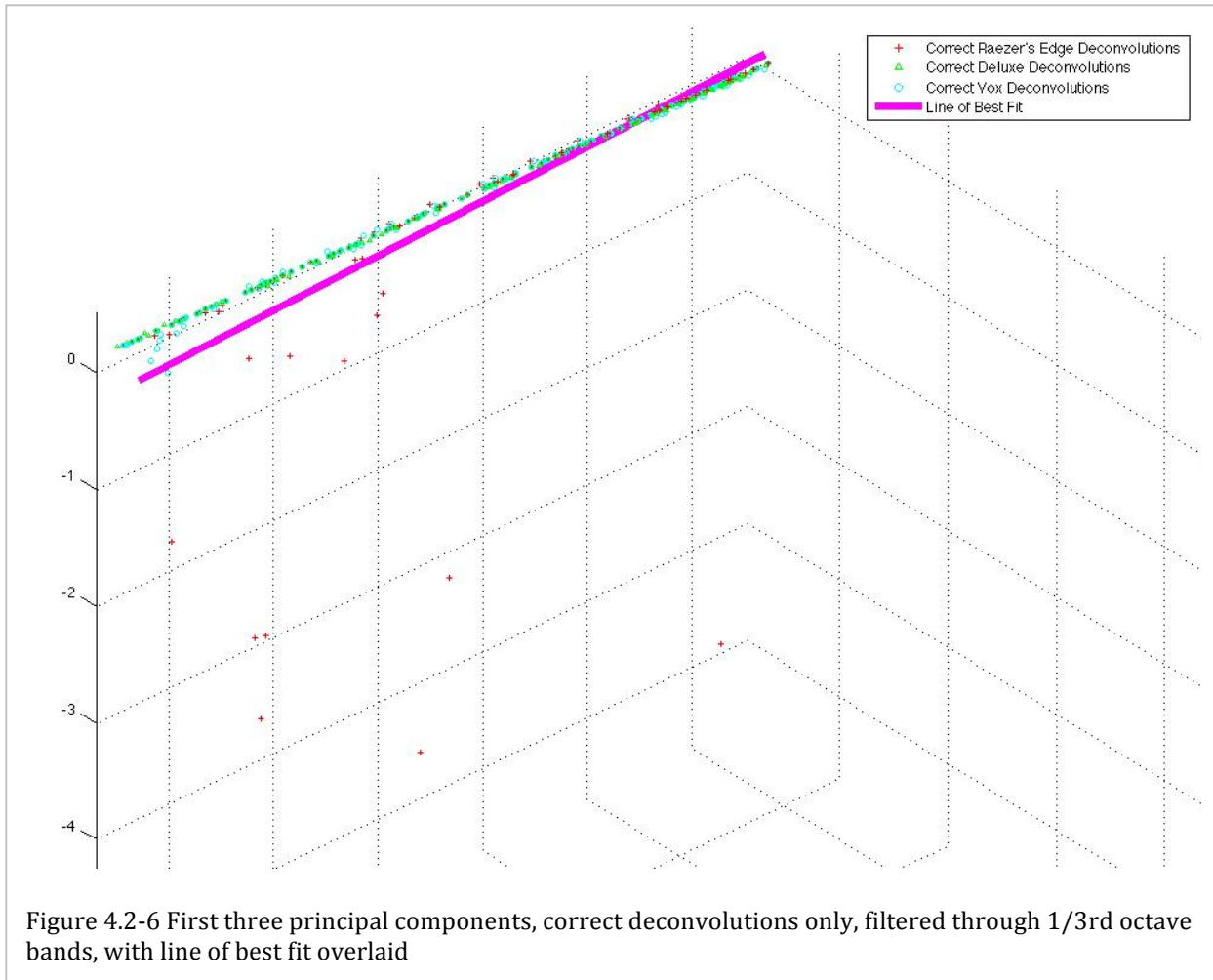


Figure 4.2-5 Plot of first three principal components obtained from PCA filtered with 1/3rd octave bands



Another interesting observation about the plots in Figures 4.2-3 though 4.2-6 is that the lines of best fit tend to become more sloped as the number of data points is reduced through filtering.

The results of amplifier identification for the test signals when measured from the training data are presented in Tables 4.2-1, 4.2-2, and 4.2-3 below. These tables show the results of amplifier identification for 1/12<sup>th</sup>, 1/6<sup>th</sup>, and 1/3<sup>rd</sup> octave band filters respectively.

Guitar: Les Paul  
 Comparison Method: Training Data  
 Octave Band Filter: 1/12

Sample Number	Correct Amplifier	Probability produced by algorithm			Correct Selection
		Raezer's Edge	Fender Deluxe	Vox	
1	Vox Valvetronix	81.41	41.66	76.93	No
2	Raezer's Edge	72.26	44.98	82.75	No
3	Fender Deluxe	75.34	75.48	49.19	Yes
4	Vox Valvetronix	76.70	47.15	76.15	No
5	Vox Valvetronix	81.41	41.66	76.93	No
6	Vox Valvetronix	70.96	47.36	81.67	Yes
7	Vox Valvetronix	81.41	41.66	76.93	No
8	Raezer's Edge	72.26	44.98	82.75	No
9	Fender Deluxe	75.34	75.48	49.19	Yes
10	Vox Valvetronix	76.70	47.15	76.15	No
11	Vox Valvetronix	81.41	41.66	76.93	No
12	Fender Deluxe	64.45	52.83	82.72	No
13	Raezer's Edge	79.85	48.97	71.18	Yes
14	Vox Valvetronix	87.25	43.72	69.03	No
15	Vox Valvetronix	70.96	47.36	81.67	Yes
16	Raezer's Edge	72.26	44.98	82.75	No
17	Vox Valvetronix	70.96	47.36	81.67	Yes
18	Vox Valvetronix	72.93	44.26	82.81	Yes
19	Fender Deluxe	56.36	92.56	51.08	Yes
20	Raezer's Edge	72.26	44.98	82.75	No
Percentage correctly selected:					40.00%

Table 4.2-1

Guitar: Les Paul

Comparison Method: Training Data

Octave Band Filter: 1/6

Sample Number	Correct Amplifier	Probability produced by algorithm			Correct Selection
		Raezer's Edge	Fender Deluxe	Vox	
1	Vox Valvetronix	83.17	41.92	74.91	No
2	Raezer's Edge	71.87	45.48	82.64	No
3	Fender Deluxe	66.33	75.48	58.19	Yes
4	Vox Valvetronix	77.41	46.20	76.39	No
5	Vox Valvetronix	83.17	41.92	74.91	No
6	Vox Valvetronix	70.54	47.67	81.79	Yes
7	Vox Valvetronix	83.17	41.92	74.91	No
8	Raezer's Edge	71.87	45.48	82.64	No
9	Fender Deluxe	66.33	75.48	58.19	Yes
10	Vox Valvetronix	77.41	46.20	76.39	No
11	Vox Valvetronix	83.17	41.92	74.91	No
12	Fender Deluxe	61.85	51.17	86.99	No
13	Raezer's Edge	80.77	48.96	70.27	Yes
14	Vox Valvetronix	87.78	43.83	68.39	No
15	Vox Valvetronix	70.54	47.67	81.79	Yes
16	Raezer's Edge	71.87	45.48	82.64	No
17	Vox Valvetronix	70.54	47.67	81.79	Yes
18	Vox Valvetronix	76.66	43.50	79.84	Yes
19	Fender Deluxe	49.44	96.29	54.27	Yes
20	Raezer's Edge	71.87	45.48	82.64	No
Percentage correctly selected:					40.00%

Table 4.2-2

Guitar: Les Paul  
 Comparison Method: Training Data  
 Octave Band Filter: 1/3

Sample Number	Correct Amplifier	Probability produced by algorithm			Correct Selection
		Raezer's Edge	Fender Deluxe	Vox	
1	Vox Valvetronix	85.02	35.97	79.01	No
2	Raezer's Edge	70.31	38.48	91.20	No
3	Fender Deluxe	55.88	79.92	64.21	Yes
4	Vox Valvetronix	77.75	42.35	79.90	Yes
5	Vox Valvetronix	85.02	35.97	79.01	No
6	Vox Valvetronix	69.84	46.91	83.26	Yes
7	Vox Valvetronix	85.02	35.97	79.01	No
8	Raezer's Edge	70.31	38.48	91.20	No
9	Fender Deluxe	55.88	79.92	64.21	Yes
10	Vox Valvetronix	77.75	42.35	79.90	Yes
11	Vox Valvetronix	85.02	35.97	79.01	No
12	Fender Deluxe	66.46	47.04	86.50	No
13	Raezer's Edge	81.28	46.13	72.60	Yes
14	Vox Valvetronix	87.18	39.97	72.85	No
15	Vox Valvetronix	69.84	46.91	83.26	Yes
16	Raezer's Edge	70.31	38.48	91.20	No
17	Vox Valvetronix	69.84	46.91	83.26	Yes
18	Vox Valvetronix	73.90	44.35	81.76	Yes
19	Fender Deluxe	48.14	95.58	56.28	Yes
20	Raezer's Edge	70.31	38.48	91.20	No
Percentage correctly selected:					50.00%

Table 4.2-3

The best performing identification occurred using 1/3<sup>rd</sup> octave band filtering when using the distance between the test data points and the training data line of best fit. However, this method produced only 50% correctness.

#### 4.3. Testing data results (Method Two)

The first amplifier identification method using the training data revealed the pattern of linearity that exists within the correct deconvolutions; however, the second method

produced much more accurate and reliable results. After passing the test samples through the same pre- and post-processing steps as the training data, the pattern of linearity of correct deconvolutions versus a wide scattering of data points for the incorrect deconvolutions remained consistent across 1/3<sup>rd</sup>, 1/6<sup>th</sup>, and 1/12<sup>th</sup> octave band filters. Figures 4.3-1, 4.3-2, and 4.3-3 show plots of the PCA results for a test data sample at 1/3<sup>rd</sup>, 1/6<sup>th</sup>, and 1/12<sup>th</sup> octave bands.

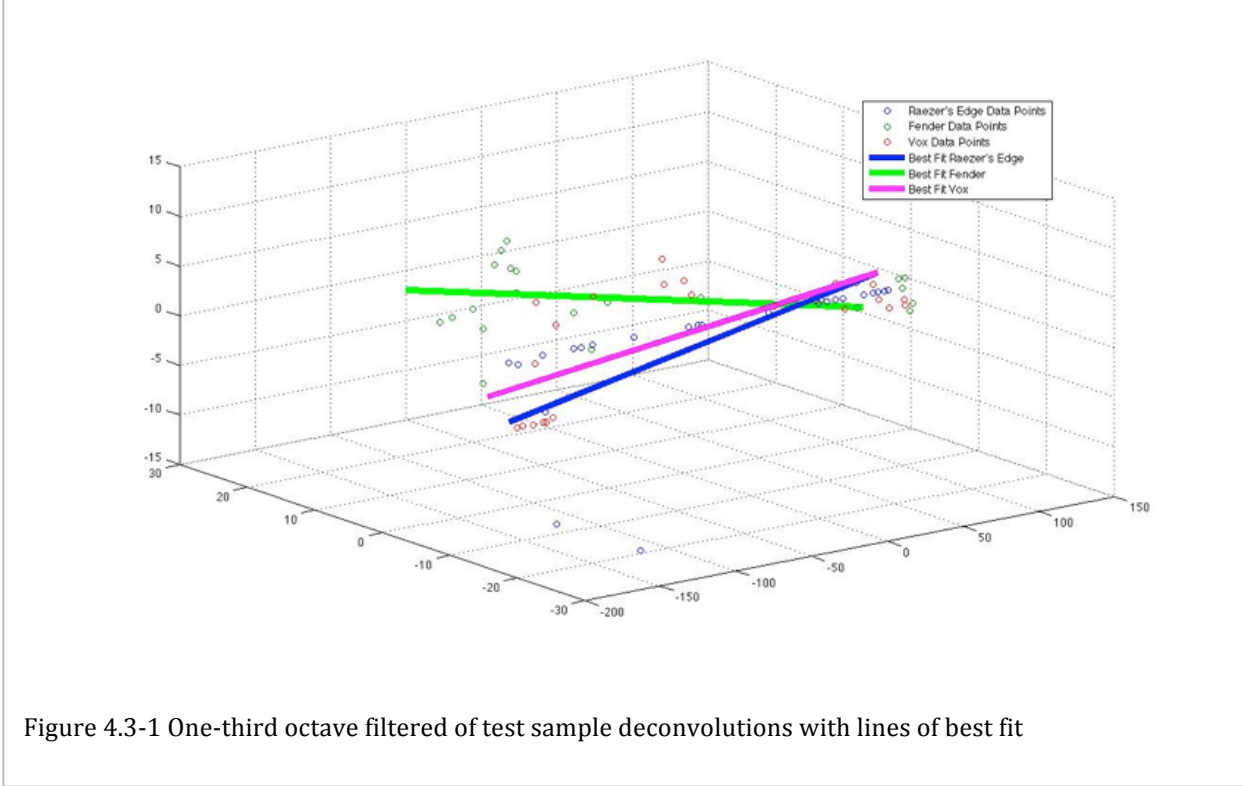


Figure 4.3-1 One-third octave filtered of test sample deconvolutions with lines of best fit

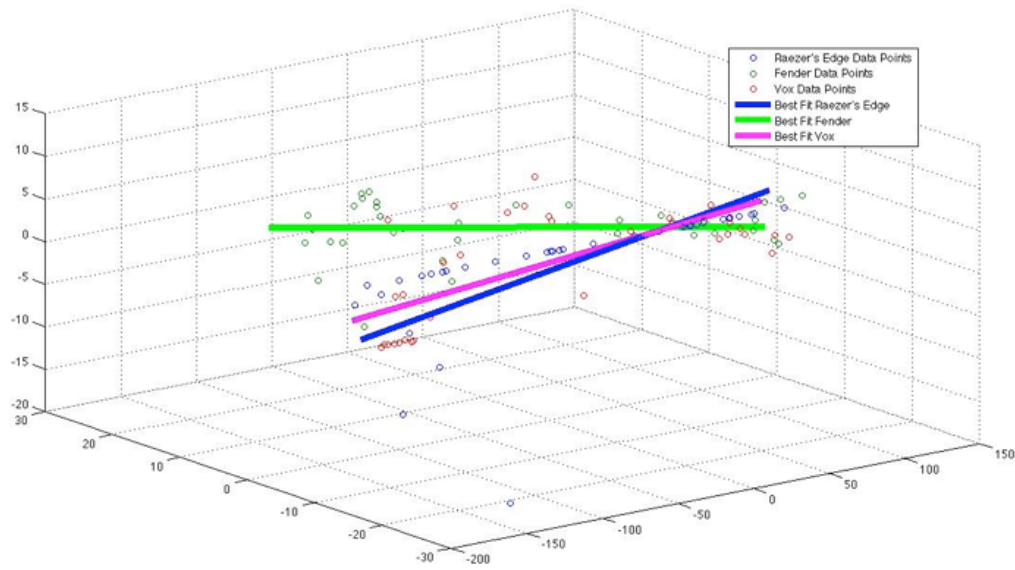


Figure 4.3-2 One-sixth octave filtered deconvolutions of test sample with lines of best fit

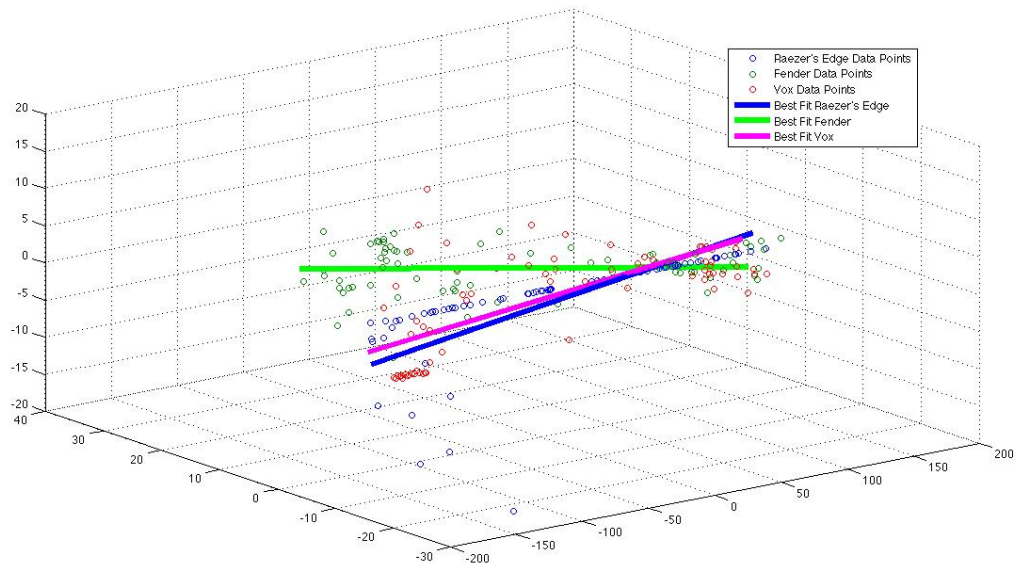


Figure 4.3-3 One-twelfth octave filtered deconvolutions of test sample with lines of best fit

Figures 4.3-1, 4.3-2, and 4.3-3 show the lines of best fit for a single sample of the testing data (sample number 20). In this particular example, the correct amplifier was the Raezer's Edge as can be seen below in Tables 4.3-1, 4.3-2, and 4.3-3. In Figure 4.3-3 showing the 1/12<sup>th</sup> filtered deconvolutions, the blue line of best fit appears more in line with the actual data points. However, it is not exactly covering the Raezer's Edge data points because of the few outliers that are far off from the line. This imperfect line is also reflected in the percentage of certainty for the Raezer's Edge in this example (73.10% certainty vs. 71.00% for the Vox and 55.90% for the Fender).

In other examples, the plots are much cleaner with the line of best fit almost completely covering the data points for the correct amplifier. Rather than showing more plots of the best-fit lines for the testing data, Tables 4.3-1, 4.3-2, and 4.3-3 show the identification results with percentages of certainty. Where these percentages for the correct amplifier are much higher than the other two amplifier percentages, the plots for those examples would show clear and well-aligned best-fit lines that almost completely cover all data points for the correct amplifier.

Guitar: Les Paul  
 Comparison Method: Self  
 Octave Band Filter: 1/12

Sample Number	Correct Amplifier	Probability produced by algorithm			Correct Selection
		Raezer's Edge	Fender Deluxe	Vox	
1	Vox Valvetronix	71.74	50.67	77.59	Yes
2	Raezer's Edge	73.10	55.90	71.00	Yes
3	Fender Deluxe	58.22	73.55	68.23	Yes
4	Vox Valvetronix	65.70	53.84	80.46	Yes
5	Vox Valvetronix	71.74	50.67	77.59	Yes
6	Vox Valvetronix	70.54	51.33	78.13	Yes
7	Vox Valvetronix	71.74	50.67	77.59	Yes
8	Raezer's Edge	73.10	55.90	71.00	Yes
9	Fender Deluxe	58.22	73.55	68.23	Yes
10	Vox Valvetronix	65.70	53.84	80.46	Yes
11	Vox Valvetronix	71.74	50.67	77.59	Yes
12	Fender Deluxe	62.34	69.08	68.58	Yes
13	Raezer's Edge	78.42	56.23	65.35	Yes
14	Vox Valvetronix	66.91	52.79	80.30	Yes
15	Vox Valvetronix	70.54	51.33	78.13	Yes
16	Raezer's Edge	73.10	55.90	71.00	Yes
17	Vox Valvetronix	70.54	51.33	78.13	Yes
18	Vox Valvetronix	68.81	52.10	79.09	Yes
19	Fender Deluxe	61.71	69.41	68.87	Yes
20	Raezer's Edge	73.10	55.90	71.00	Yes
Percentage correctly selected:					100.00%

Table 4.3-1

The 1/6<sup>th</sup> and 1/3<sup>rd</sup> filtered deconvolutions shown in Figures 4.3-1 and 4.3-2 above have best-fit lines that are even less well aligned with the data points. Tables 4.3-2 and 4.3-3 below contain the amplifier identification results and percentages for 1/6<sup>th</sup> and 1/3<sup>rd</sup> octave bands, similar to the 1/12<sup>th</sup> octave band in Table 4.3-1 above.

Guitar: Les Paul  
 Comparison Method: Self  
 Octave Band Filter: 1/3

Sample Number	Correct Amplifier	Probability produced by algorithm			Correct Selection
		Raezer's Edge	Fender Deluxe	Vox	
1	Vox Valvetronix	77.75	49.71	72.54	Yes
2	Raezer's Edge	67.23	55.03	77.74	No
3	Fender Deluxe	60.03	66.46	73.51	No
4	Vox Valvetronix	68.73	52.85	78.41	Yes
5	Vox Valvetronix	77.75	49.71	72.54	No
6	Vox Valvetronix	75.09	49.92	75.00	No
7	Vox Valvetronix	77.75	49.71	72.54	No
8	Raezer's Edge	67.23	55.03	77.74	No
9	Fender Deluxe	60.03	66.46	73.51	No
10	Vox Valvetronix	68.73	52.85	78.41	Yes
11	Vox Valvetronix	77.75	49.71	72.54	No
12	Fender Deluxe	71.26	58.97	69.76	No
13	Raezer's Edge	77.73	52.77	69.50	Yes
14	Vox Valvetronix	73.10	52.07	74.82	Yes
15	Vox Valvetronix	75.09	49.92	75.00	No
16	Raezer's Edge	67.23	55.03	77.74	No
17	Vox Valvetronix	75.09	49.92	75.00	No
18	Vox Valvetronix	74.28	51.02	74.70	Yes
19	Fender Deluxe	66.82	60.99	72.19	No
20	Raezer's Edge	67.23	55.03	77.74	No
Percentage correctly selected:					30.00%

Table 4.3-2

Guitar: Les Paul  
 Comparison Method: Self  
 Octave Band Filter: 1/6

Sample Number	Correct Amplifier	Probability produced by algorithm			Correct Selection
		Raezer's Edge	Fender Deluxe	Vox	
1	Vox Valvetronix	74.48	48.96	76.56	Yes
2	Raezer's Edge	68.82	55.97	75.21	No
3	Fender Deluxe	63.74	68.60	67.65	Yes
4	Vox Valvetronix	65.83	53.73	80.44	Yes
5	Vox Valvetronix	74.48	48.96	76.56	Yes
6	Vox Valvetronix	72.00	49.83	78.17	Yes
7	Vox Valvetronix	74.48	48.96	76.56	Yes
8	Raezer's Edge	68.82	55.97	75.21	No
9	Fender Deluxe	63.74	68.60	67.65	Yes
10	Vox Valvetronix	65.83	53.73	80.44	Yes
11	Vox Valvetronix	74.48	48.96	76.56	Yes
12	Fender Deluxe	66.98	64.33	68.68	No
13	Raezer's Edge	78.24	54.26	67.50	Yes
14	Vox Valvetronix	69.04	51.99	78.97	Yes
15	Vox Valvetronix	72.00	49.83	78.17	Yes
16	Raezer's Edge	68.82	55.97	75.21	No
17	Vox Valvetronix	72.00	49.83	78.17	Yes
18	Vox Valvetronix	73.89	51.83	74.28	Yes
19	Fender Deluxe	71.91	55.83	72.27	No
20	Raezer's Edge	68.82	55.97	75.21	No
Percentage correctly selected:					70.00%

Table 4.3-3

In the Tables above, the incorrect identifications are consistent between 1/3<sup>rd</sup> octave filtering and 1/6<sup>th</sup> octave filtering. It can be seen that as more granular filtering is applied with 1/6<sup>th</sup> octave bands, several of the incorrect identification in the 1/3<sup>rd</sup> table are correctly identified in the 1/6<sup>th</sup> table causing the correct percentage to jump from 30% to 70%. Moving to 1/12<sup>th</sup> octave filtering improves the identification precision even further to 100% for these twenty samples. The reason for this improvement is a dilution of the effect of the outliers on the standard deviation from the line of best fit.

The final test performed using these data processing methods involved samples from a different guitar. This final test was meant as a further proof of concept that these methods can be used for accurate guitar amplifier identification from a blindly convolved signal. The amplifier identification results from the Telecaster samples are presented in Table 4.3-4.

Guitar: Telecaster Comparison Method: Self Octave Band Filter: 1/12					
Sample Number	Correct Amplifier	Probability produced by algorithm			Correct Selection
		Raezer's Edge	Fender Deluxe	Vox	
1	Raezer's Edge	95.31	48.45	56.24	Yes
2	Raezer's Edge	92.14	47.52	60.34	Yes
3	Fender Deluxe	60.35	69.70	69.95	No
4	Vox Valvetronix	68.12	51.35	80.52	Yes
Percentage correctly selected:					75.00%

Table 4.3-4

The percentages shown in Table 4.3-4 suggest that the amplifier identification algorithm performed even better for the Telecaster than it did for the Les Paul. Although the overall percentage of correct selections is lower than the 1/12<sup>th</sup> octave results for the Les Paul, the overall confidence displayed for each correct selection is much higher for the Telecaster than the Les Paul. In sample number three, the Vox was incorrectly chosen. However, the Vox was only 0.25% higher than the actual correct amplifier. In the other three cases, the correct amplifier was chosen with around 30% higher confidence than the second highest percentage. A more robust set of data for the Telecaster (and other guitars) would need to be created in order to confirm these assumptions, but this test and the

results shown in Table 4.3-4 suggest that this amplifier identification technique would be extensible to any guitar input.

## 5. Discussion

### 5.1. Training data results served as a discovery method

The creation of the training data set and the processing methods applied to it were invaluable for the discovery of the linearity feature in the correct deconvolutions and the wide scattering of the incorrect deconvolutions. Even though the test signals did not always line up properly with the training set, it is still noteworthy that correct identifications were made no less than 40% of the time. This fact is interesting because the actual signals that were used consisted of completely different musical excerpts recorded at different times. Accounting for differences in the equipment calibration, tuning, and other such factors, correct amplifier identifications were still made successfully. Also, as shown in Tables 4.2-1, 4.2-2, and 4.2-3 there was consistency between the incorrect identifications in all three of the filtering scenarios (i.e., the same samples were incorrect in the 1/12<sup>th</sup>, 1/6<sup>th</sup>, and 1/3<sup>rd</sup> octave bands except that there were two more successful identifications in the 1/3<sup>rd</sup> octave case).

It is not exactly clear why the 1/3<sup>rd</sup> octave band filtering performed the best in the case of Method One. The higher identification precision was most likely because 1/3<sup>rd</sup> octave band filtering reduces the data points, and fewer data points for comparison gives greater weight to each data point. For the incorrect deconvolutions, the greater weight on the scattered data points most likely caused the orthogonal distances of the averages from the line of best fit to increase, whereas the correct deconvolutions would have had more data points in a smaller area near the best-fit lines.

This method was ultimately underwhelming, as it did not produce reliable results. However, the analysis of the PCA plot of all of the deconvolutions first revealed the linearity pattern. When the test data best-fit lines were overlaid onto the training set, often the line of best fit intersected the best-fit line for the training data. The orientation of the test data on the three-dimensional hyperplane was different from the training, and this ultimately led to incorrect identifications. Though the majority of identifications were incorrect for this method, it was easily observable that the test data also always displayed the correct deconvolutions in a linear pattern.

## 5.2. Linearity as deciding factor

The second method for amplifier identification proposed in this study was able to consistently determine the correct amplifiers with a high confidence through determining linearity.

From the analysis of all data set deconvolutions, the relatively low noise in the correct deconvolutions when compared to the incorrect ones led to strong linear clustering when PCA was performed. The incorrect deconvolutions always exhibited a tendency of widely scattered points in the filtered data.

The most illuminating step in the methods presented in this work occurred after PCA was performed. Without PCA and subsequent three-dimensional plotting, the linearity of the correct deconvolutions would not have been obvious. After PCA was performed and the results were plotted, it became clear that the amplifier identification methods should be based on a measure of linearity in the correct deconvolutions versus scattering in the

incorrect ones. Prior to this step, it was still unclear how any identification would be made with any sort of consistent accuracy.

The method used for measuring “correctness” could possibly be improved by using other statistical calculations besides standard deviation from the line of best fit such as an average orthogonal distance, or a calculated correlation. However, this method did produce reliable results for the 1/12<sup>th</sup> octave band. Perhaps other methods might improve the identification accuracy at 1/6<sup>th</sup> and 1/3<sup>rd</sup> octave bands, but the accuracy of the 1/12<sup>th</sup> bands was sufficient as a prototype for further research.

### **5.3. Identification is based on individual output; not a secondary data set**

It became apparent through testing that how the test data correlated with the training data was much less significant for correct amplifier identification than the linearity of correct deconvolutions versus non-linearity of incorrect deconvolutions within each test. When the data for all three deconvolutions from a single test was projected into three dimensions, the correct amplifier was obvious to the naked eye, even in the 1/3<sup>rd</sup> octave band case.

An efficient dataset is key to the extensibility of this research towards future applications. A single, self-comparing dataset enables accurate identification, and the use of this single dataset reduces the amount of processing time, data collection, and disk space required to store all of the data. Patterns emerge from self-comparison regardless of the guitar used, as shown in the Fender Telecaster results, rendering use of a first, training dataset unnecessary.

#### **5.4. Degree of data filtering affects accuracy**

Filtering to reduce data greatly affects the accuracy of amplifier identification. This fact was demonstrated in both amplifier identification methods. In the case of Method Two, a lower degree of filtering through octave band filters (i.e., 1/12<sup>th</sup> octave bands) led to a more accurate result, while Method One performed better with a higher degree of filtering (i.e., 1/3<sup>rd</sup> octave bands).

The use of octave band filters discretized the data by returning scalar values for each center frequency, transforming millions of data points into a computationally efficient data set. The linearity feature may not have been as apparent without this filtering step. The filtered, discrete data points allowed for easy recognition of the linear pattern that appeared with the correct deconvolutions after performing PCA.

In the case of 1/3<sup>rd</sup> octave band filters in the Method Two, the amount of data was reduced too much. The reduction of data points caused each point to carry greater weight in calculating the standard deviation from the best-fit line. The greater weight of each point also degraded the accuracy of the best-fit line by forcing the line to skew more towards the outlying data points and away from the visible linearity of the majority of data points. The 1/6<sup>th</sup> octave band filters performed admirably, increasing the precision from 30% in the case of 1/3<sup>rd</sup> octave band filters to 70%. However, the processing time to calculate the 1/6<sup>th</sup> octaves did not differ much from the processing time required for 1/12<sup>th</sup> octave bands, and the performance of the 1/12<sup>th</sup> octave band filters increased the precision to 100%.

From examining Table 4.3-1 and Table 4.3-3, the increase of data points causes percentages from the incorrect identifications to eventually cross a “threshold” and become

correct. In each case, the incorrect identifications moved from “very incorrect” in the 1/3<sup>rd</sup> case, to “mostly correct” in the 1/6<sup>th</sup> case, and finally to “completely correct”.

The 1/12<sup>th</sup> octave band filters allowed for a much crisper line of best fit that lined up well when overlaid with the individual data points. Even with 1/12<sup>th</sup> octave band filtering, the best-fit lines did not always lie exactly over all of the data points in many cases. With more data points, the effects from the far outliers on the standard deviation were reduced. With the reduced amount of data from the 1/6<sup>th</sup> and 1/3<sup>rd</sup> octave filters, the outliers have a larger effect and cause inaccuracy in the estimation. The 1/12<sup>th</sup> octave band filtered data contained enough data points close to the best-fit lines to reduce the influence of the outliers on the analysis and allow for accurate amplifier identification.

The standard deviation from the lines of best fit appears to be inversely proportional to the number of data points used in each measurement. As the number of data points decreases due to wider octave band filters, there is less precision for each data point. Furthermore, the outliers have a much stronger influence on the fitness of the line. This effect can be seen in Figure 4.3-1. The blue line represents the best-fit line for the Raezer's Edge. While most of the data points fall into a relatively narrow region, there are two points that fall far away from the others. These points force the line of best fit to move away from the other points, and this effect ultimately leads to an incorrect choice in this instance.

## 6. Conclusions and Future Work

This thesis provides a promising approach for determining amplifier models from recorded audio. More research and collection of additional data could expand upon these findings and open application possibilities.

Further research would require a system using many more amplifiers, microphone capsule locations at various distances from the amplifiers, and more guitar samples from different guitar models. Additional data from more instruments and locations would lead to the creation of a more realistically useful platform by allowing users to perform amplifier identification using a large number of realistic scenarios. The first step towards creating such a robust system would be the collection of face plane data for many more amplifiers. An amplifier bank containing face plane data for tens to hundreds of amplifiers would be necessary to cover the wide range of possibilities that musicians and engineers currently have access to.

Because many engineers place microphones close to the center face of the amplifier, these results are useful. However, these cover only a narrow spatial location around the center of the speaker at a distance of two inches. Thus, it cannot yet be generalized to situations where the microphone is placed anywhere other than two inches from the center face of the amplifier. Impulse responses for multiple planes of the three amplifiers included here have been measured, as mentioned in Matthew and Blackmore (2013) and Matthew (2012). This data could be processed in the same ways as the face plane measurements for a logical next step in this type of research. Assuming that similar results are obtained, impulse responses for many more amplifiers would need to be measured.

Further research makes this study more commercially applicable and useful. This future work would enable commercial application of the research in this thesis, as it would provide practitioners with tools to determine how to achieve a desired sound during recording or live musical performances.

In addition to more robust data, it would be interesting to test how much confidence could be attained using even more granular filtering such as 1/24<sup>th</sup> or 1/36<sup>th</sup> band octave filters. However, the processing time involved with using these filters would most likely outweigh any benefits to accuracy. The twenty small guitar samples used in this study still required overnight processing for the 1/12<sup>th</sup> band octave filters. Even more filters with more data would greatly slow down the system, so the benefits of using such a large number of octave band filters would first need to be quantified.

The results reveal how each model sounds at specific spatial locations in front of and very close to the amplifiers. Microphone type and placement around an amplifier plays a significant role in the overall spectrum of the captured sound. With more data at different locations around each amplifier, this work could be easily extended to provide information about spectral characteristics and radiation pattern differences between amplifiers, and that information could be used with the same processing techniques presented in this study to determine amplifier models at multiple locations.

An expanded data set encompassing multiple amplifiers, locations, and microphones would provide recording engineers and musicians with powerful tools for achieving their creative goals. The ability to “deconstruct” prior recordings would be helpful for both novice and experienced recording engineers. Decisions on instrument selection and

microphone placement could then be informed by the analysis of desired sonic characteristics from previously recorded material.

This thesis presented a promising set of results for instrument model identification from recorded material. The results of the small data sets studied justify an expanded approach using much more data to create a viable commercial product.

## 7. Works Referenced

- Bissinger, George. "Structural Acoustics of Good and Bad Violins." *Journal of the Acoustical Society of America* 124.3 (2008): 1764-1773.
- Boren, Braxton, and Agnieszka Roginska. "Multichannel Impulse Response Measurement in Matlab." Audio Engineering Society: 131th Convention. New York. Oct 2011.
- Brown, J., Houix, O., and S. McAdams. "Feature Dependence in the Automatic Identification of Musical Woodwind Instruments." *Journal of the Acoustical Society of America*. 109.3 (2001): 1064-1072. Online.
- Eronen, A., and A. Klapuri. "Musical instrument recognition using cepstral coefficients and temporal features." *Acoustics, Speech, and Signal Processing, 2000. ICASSP '00. Proceedings. 2000 IEEE International Conference*. Vol.2: II753-II756.  
URL: <http://ieeexplore.ieee.org/stamp/stamp.jsp?tp=&arnumber=859069&isnumber=18644>
- Fillinger, L., Sutin, A., and A. Sedunov, "Cross-correlation of ship noise for water traffic monitoring," *Proceedings of the Journal of the Acoustical Society of America*. 126.4, pt. 2, 2251, 2009. <http://asa.aip.org/web2/asa/abstracts/search.oct09/asa421.html>
- Fritz, C., Curtin, J., Poitevineau, J., Morrel-Samuels,P., and F. Tao. "Player Preferences Among New and Old Violins." *PNAS*. 109.3 (2012): 760-763.
- Logan, Beth. "Mel Frequency Cepstral Coefficients for Music Modeling." *Proceedings of the ISMIR International Symposium on Music Information Retrieval*. Plymouth, MA: 2000.
- Madden, Andrew. *Auralization of Microphone Placement for the Recording of a Fender Deluxe Amplifier*. MM Thesis. New York University, New York, NY, 2012.
- Mairaj, Aamir. "Detection and Identification of an Aircraft by Processing Its Acoustic Signature." *2011 International Conference on Network and Electronics Engineering IPCSIT*. Vol11: 2011.
- Matthew, Justin. *An Analysis of Measuring and Computing the Radiation Patterns of Electric Guitar Amplifiers*. MM Thesis. New York University, New York, NY, 2012.
- Matthew, J. and S. Blackmore. "Radiation Pattern Differences Between Electric Guitar Amplifiers." Audio Engineering Society: 134th Convention. Rome, Italy. May 2013.
- McAdams, S. and A. Bregman "Hearing Musical Streams". *Computer Music Journal* 3.4 (1979):26-43, 60.

- Patil, K., Pressnitzer, D., Shamma, S., and M. Elhilali. "Music in Our Ears: The Biological Bases of Musical Timbre Perception". *PLoS Comput Biol* 8.11:e1002759. doi:10.1371/journal.pcbi.1002759. <http://www.ploscompbiol.org/article/info%3Adoi%2F10.1371%2Fjournal.pcbi.1002759#s1>
- Plassmann, H., O'Doherty, J., Shiv, B., and A. Rangel. "Marketing Actions Can Modulate Neural Representations of Experienced Pleasantness." *PNAS*. 105.3 (2008): 1050-1054.
- Press, W., Teukolsky, S., Vetterling, W., and B. Flannery. "Convolution and Deconvolution Using the FFT." *Numerical Recipes in C: The Art of Scientific Computing*. 2nd Edition. Cambridge: Cambridge University Press, 1992. Rpt. in 9.29/9.912 (BCS) & 8.261 (Physics) *Introduction to Computational Neuroscience Online Course Readings*. Sebastian Seung, 2004. <http://hebb.mit.edu/courses/9.29/2004/readings/c13-1.pdf>
- Rabiner, L. and R. Schafer. *Digital Processing of Speech Signals*. Upper Saddle River, NJ: Prentice Hall. 1978. Print.
- Roads, Curtis. *The Computer Music Tutorial*. Massachusetts Institute of Technology Press, Cambridge, MA, 1996. Print.
- Roginska, A., Case, A., Madden, A., and J. Anderson. "Measuring Spectral Directivity of an Electric Guitar Amplifier." Audio Engineering Society: 132nd Convention. Budapest, Hungary. April 2012.
- Roginska, A., Matthew J., Madden, A., Anderson, J., and A. Case. "Measurement and Analysis of the Spectral Directivity of an Electric Guitar Amplifier: Vertical Plane." Audio Engineering Society: 133rd Convention. San Francisco, CA, USA. October 2012.
- Schiens, Jonathan. "A Tutorial on Principal Component Analysis, Version 3.01." New York University, 2009. <http://www.snl.salk.edu/~shlens/pca.pdf>
- Stafford, Roger. "Linear Regression in 3D Data Points." Matlab Newsgroup. 15 Mar 2005. [http://www.mathworks.com/matlabcentral/newsreader/view\\_thread/90452](http://www.mathworks.com/matlabcentral/newsreader/view_thread/90452)
- Stockham, Thomas. "Restoration of Old Recordings by Means of Digital Signal Processing," Audio Engineering Society: 41st Convention. October, 1971. Audio Engineering Society reprint 831 (D-4).
- Stockham, T., Cannon, T., and R. Ingebretsen. "Blind deconvolution through digital signal processing," *Proceedings of the IEEE*. 63.4 (1975): 678- 692.
- Whalen, Anthony D. *Detection of Signals in Noise*, New York: Academic Press, 1971. Print.

## Appendix

### 7.1. Spectral plots of face plane outputs

The following charts depict deconvolutions from each amplifier's deconvolution array across 6 octaves of the notes A and C.

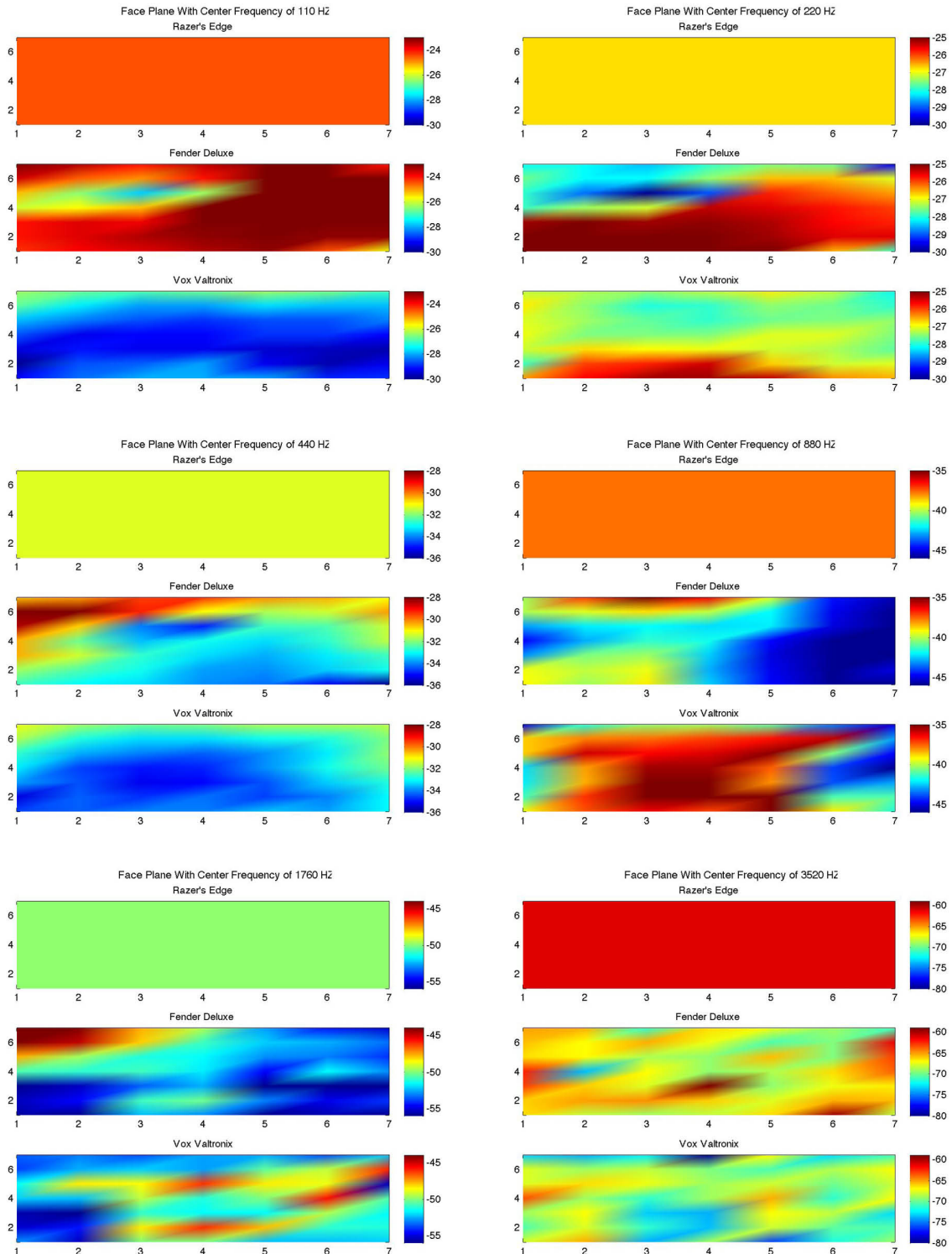


Figure 7.1-1 Deconvolutions from the Raezer's Edge deconvolution array across 6 octaves of A. In this example, the Raezer's Edge was the correct deconvolution, and the other two amplifiers were incorrect. The Raezer's Edge is the middle amplifier in each of the six plots.

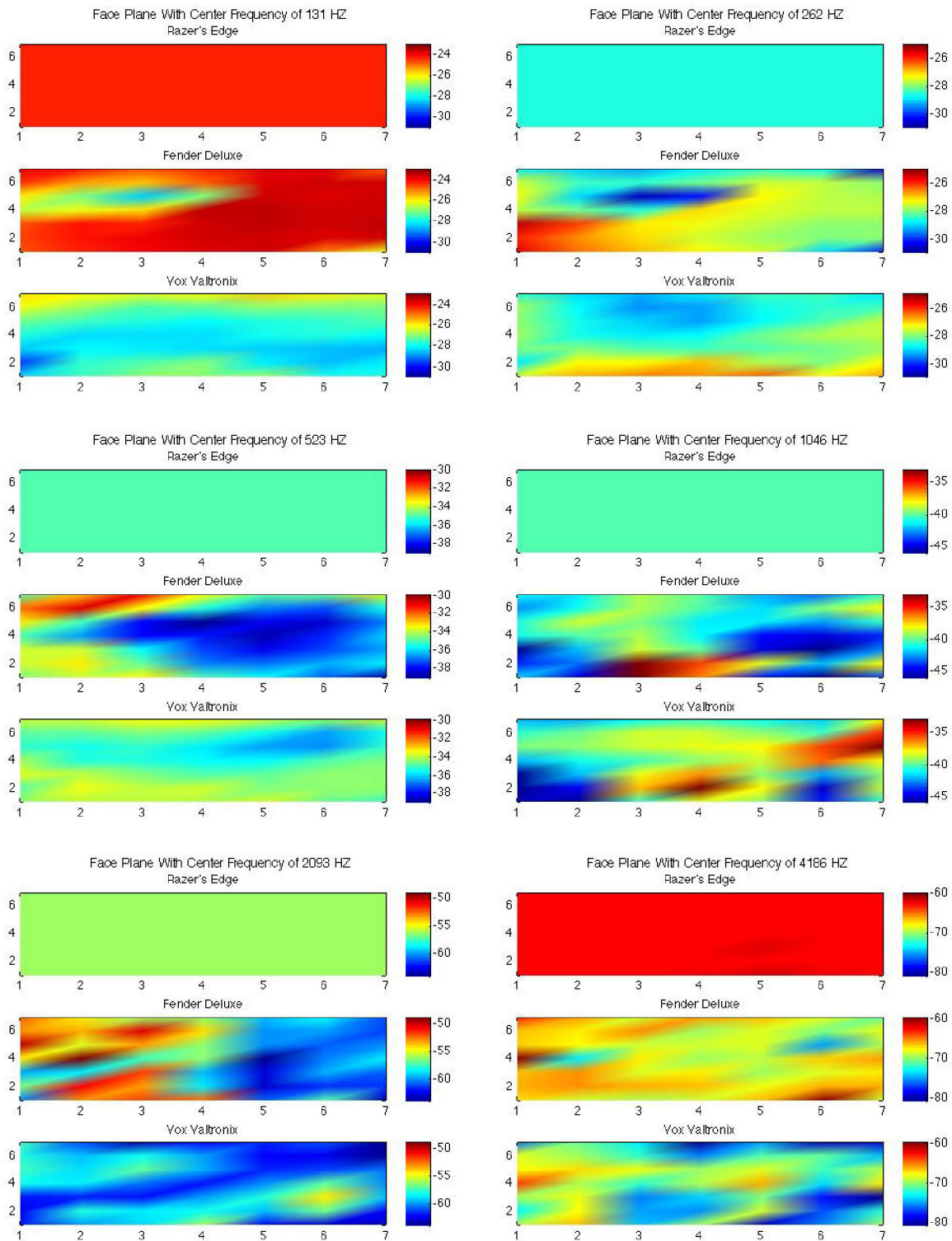


Figure 7.1-2 Deconvolutions from the Raezer's Edge deconvolution array across 6 octaves of C. In this example, the Raezer's Edge was the correct deconvolution, and the other two amplifiers were incorrect. The Raezer's Edge is the middle amplifier in each of the six plots.

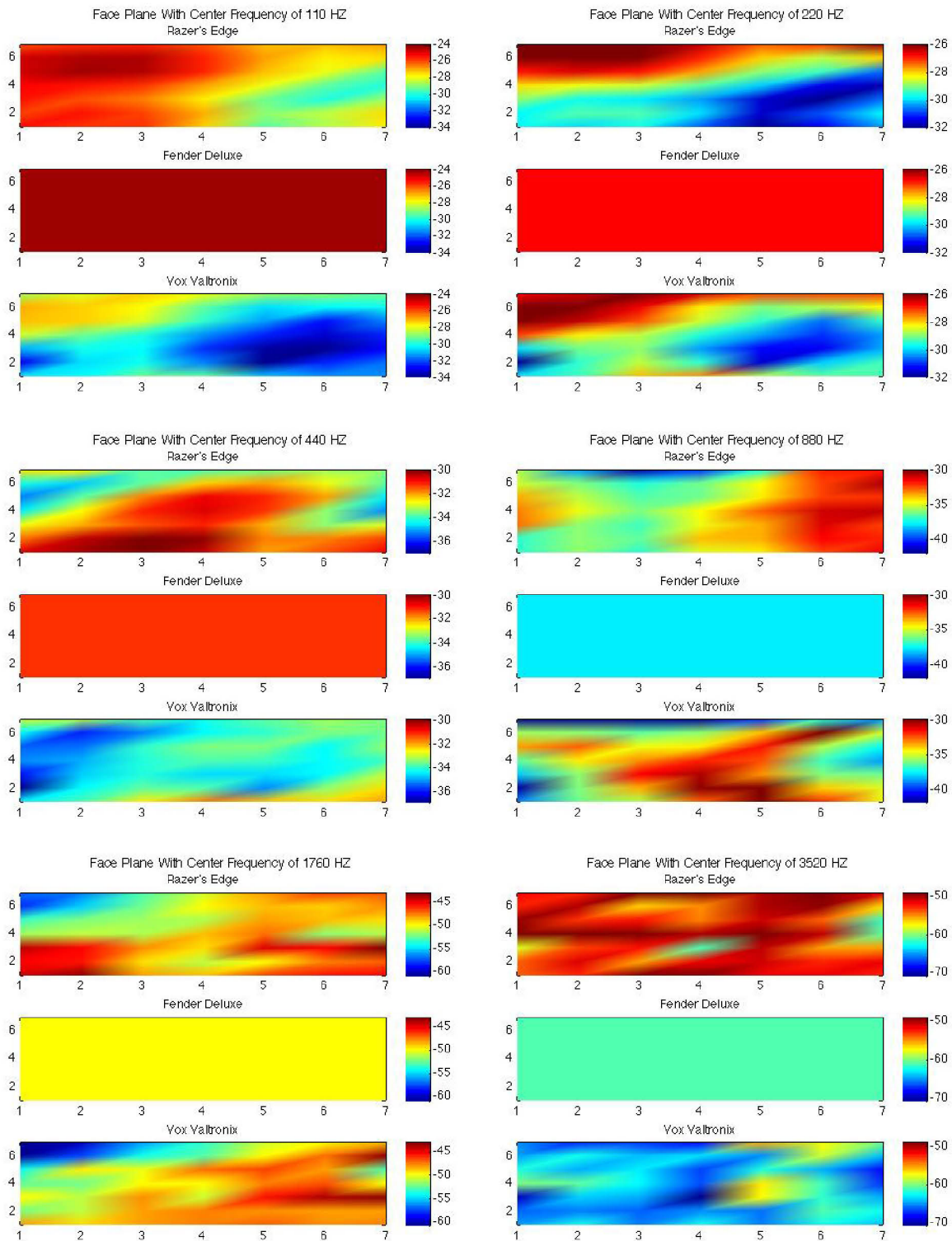


Figure 7.1-3 Deconvolutions from the Fender Deluxe deconvolution array across 6 octaves of A. In this example, the Deluxe was the correct deconvolution, and the other two amplifiers were incorrect. The Deluxe is the middle amplifier in each of the six plots.

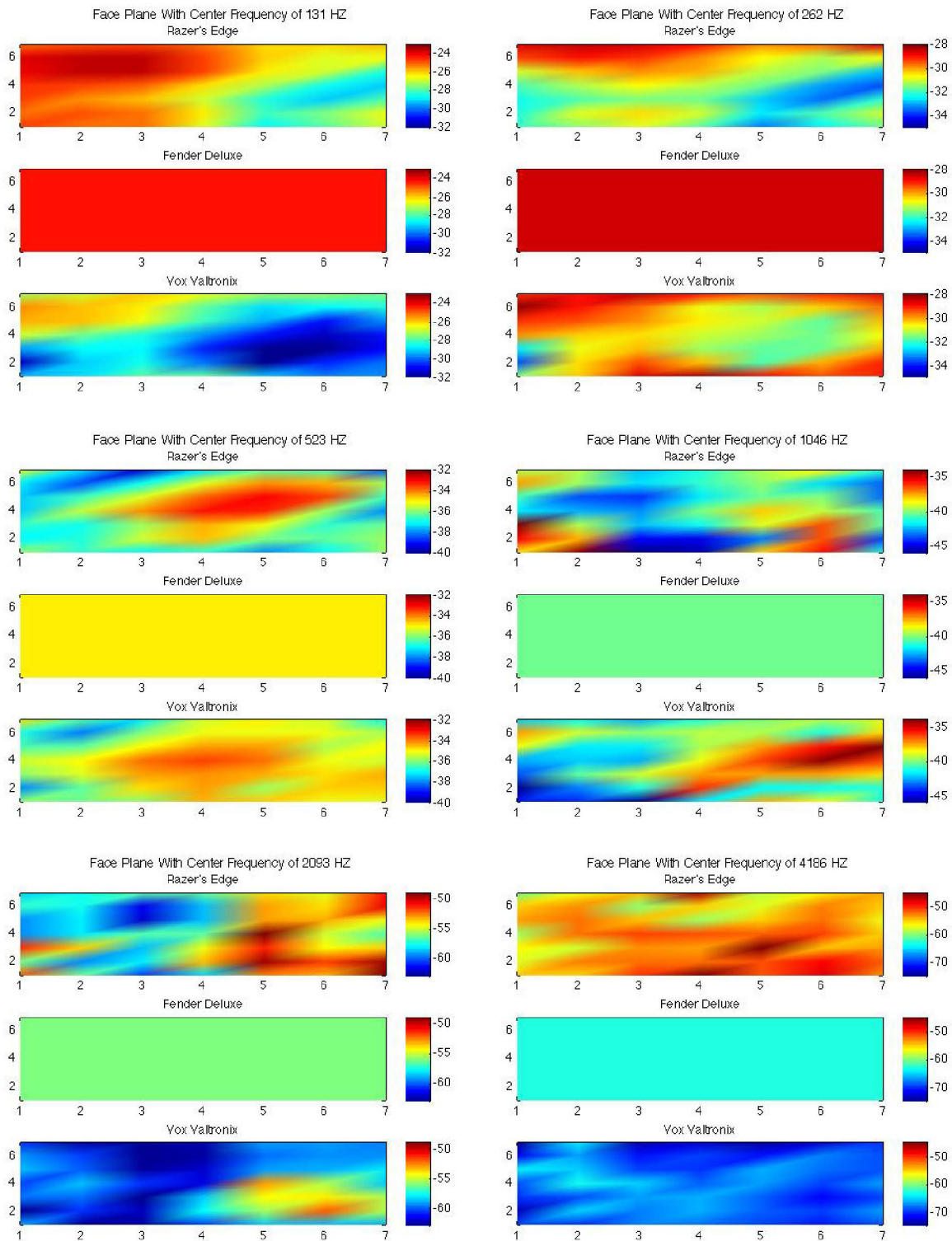


Figure 7.1-4 Deconvolutions from the Fender Deluxe deconvolution array across 6 octaves of C. In this example, the Deluxe was the correct deconvolution, and the other two amplifiers were incorrect. The Deluxe is the middle amplifier in each of the six plots.

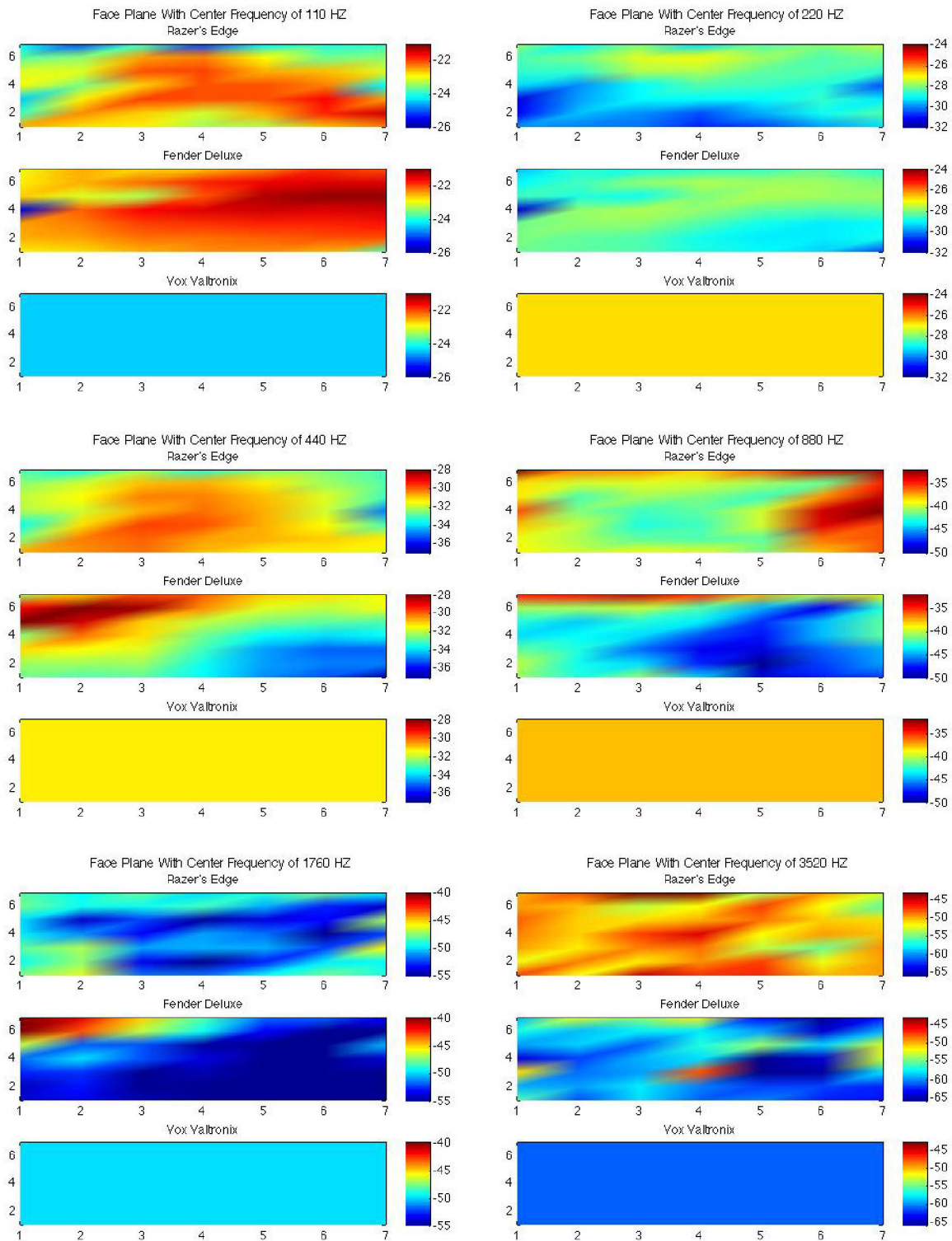


Figure 7.1-5 Deconvolutions from the Vox Valvetronix deconvolution array across 6 octaves of A. In this example, the Vox was the correct deconvolution, and the other two amplifiers were incorrect. The Vox is the middle amplifier in each of the six plots.

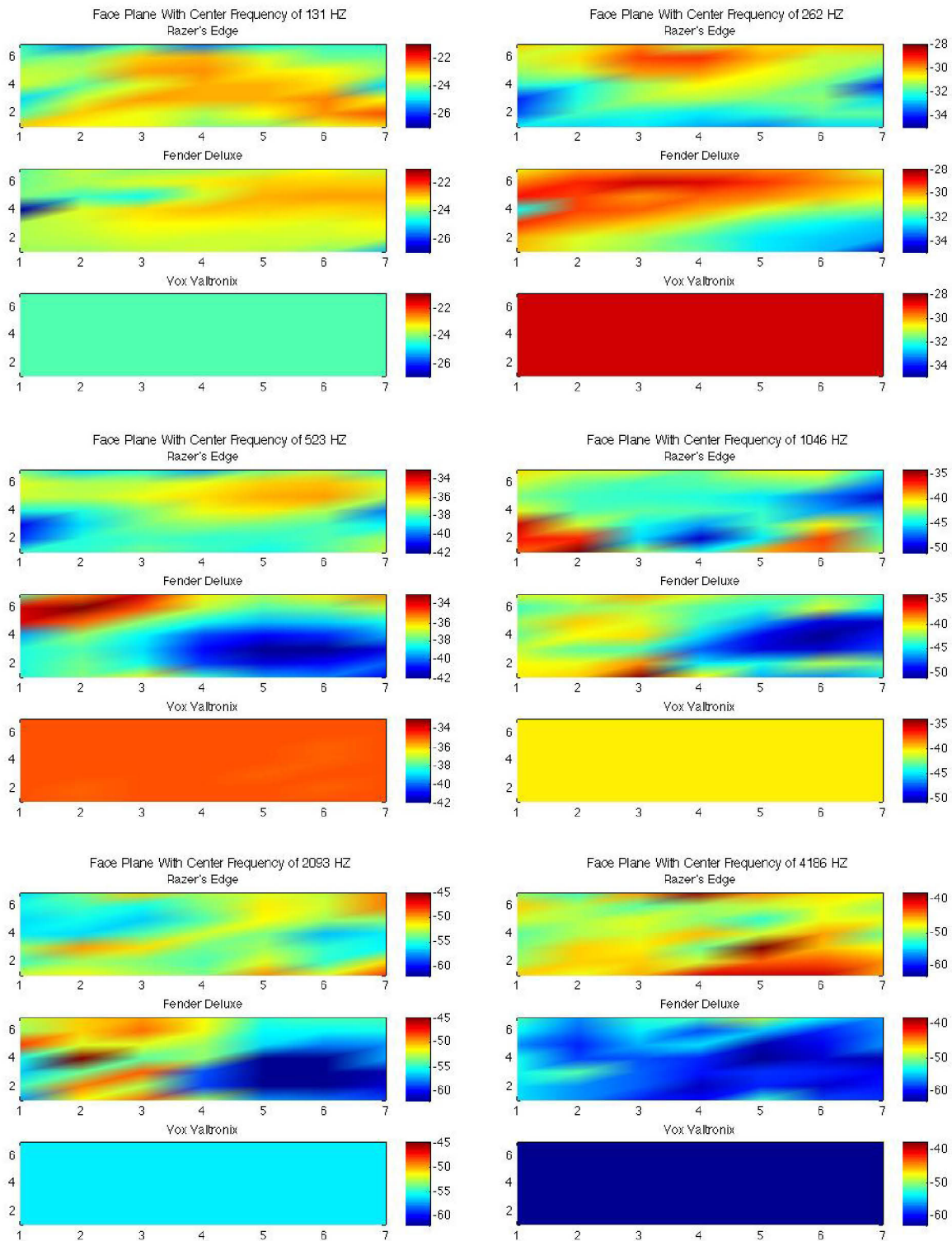


Figure 7.1-6 Deconvolutions from the Vox Valvetronix deconvolution array across 6 octaves of C. In this example, the Vox was the correct deconvolution, and the other two amplifiers were incorrect. The Vox is the middle amplifier in each of the six plots.

## 7.2. Code for best-fit line and distance calculation

1) This “best\_fit\_line.m” function comes from Stafford (2005)

```
function [m,p,s] = best_fit_line(x,y,z)

% x,y,z are n x 1 column vectors of the three coordinates
% of a set of n points in three dimensions. The best line,
% in the minimum mean square orthogonal distance sense,
% will pass through m and have direction cosines in p, so
% it can be expressed parametrically as x = m(1) + p(1)*t,
% y = m(2) + p(2)*t, and z = m(3)+p(3)*t, where t is the
% distance along the line from the mean point at m.
% s returns with the minimum mean square orthogonal
% distance to the line.
% RAS - March 14, 2005

[n,mx] = size(x); [ny,my] = size(y); [nz,mz] = size(z);
if (mx~=1)|(my~=1)|(mz~=1)|(ny~=n)|(nz~=n)
    error('The arguments must be column vectors of the same length.')
end
m = [mean(x),mean(y),mean(z)];
w = [x-m(1),y-m(2),z-m(3)]; % Use "mean" point as base
a = (1/n)*w'*w; % 'a' is a positive definite matrix
[u,d,v] = svd(a); % 'eig' & 'svd' get same eigenvalues for this matrix
p = u(:,1)'; % Get eigenvector for largest eigenvalue
s = d(2,2)+d(3,3); % Sum the other two eigenvalues
end
```

2) Code for calculation of best-fit line from return values from best\_fit\_line.m and code for calculation of orthogonal distance from this line. The following example is for 1/6th octave filtered data for the Raezer's Edge, but the same operations are applied in the 1/3rd and 1/12th case for the other two amplifiers. The only difference is the indices used to get the data from the cell arrays.

```
for j = 1:20
% load('testFilePCAScores12th');
% temp = testFilePCAScores12th{j,1};

load('testFilePCAScores6th');
temp = testFilePCAScores6th{j,1};

% 6th
[mR,pR,sR] = best_fit_line(temp(1:36,1),temp(1:36,2),temp(1:36,3));
[mD,pD,sD] = best_fit_line(temp(37:72,1),temp(37:72,2),temp(37:72,3));
[mV,pV,sV] = best_fit_line(temp(73:108,1),temp(73:108,2),temp(73:108,3));

% 6th
minXR = min(temp(1:36,1));
```

```

% put the min in terms of X
minXR = minXR*pR(2)/pR(1) - mR(1)*pR(2)/pR(1) + mR(2);
minZR = minXR*pR(3)/pR(1) - mR(1)*pR(3)/pR(1) + mR(3);

% get the maxes in terms of X
maxXR = max(temp(1:36,1));
maxYR = maxXR*pR(2)/pR(1) - mR(1)*pR(2)/pR(1) + mR(2);
maxZR = maxXR*pR(3)/pR(1) - mR(1)*pR(3)/pR(1) + mR(3);

% use the min/max to create a set of points for 3D line
xlnR = [minXR maxXR];
ylnR = [minYR maxYR];
zlnR = [minZR maxZR];

%% Calculate the distances of each point from the best-fit line

% U is the endpoint-endpoint XYZ of best fit line
uXR = maxXR - minYR;
uYR = maxYR - minYR;
uZR = maxZR - minZR;

uHatXR = uXR/sqrt(uXR^2 + uYR^2 + uZR^2);
uHatYR = uYR/sqrt(uXR^2 + uYR^2 + uZR^2);
uHatZR = uZR/sqrt(uXR^2 + uYR^2 + uZR^2);

uHatR = [uHatXR uHatYR uHatZR];

% allocate vector to hold distance for each data point to line of best fit
% for Razer
razerDistances = zeros(1,36);
% need to loop through all Razer values from the test data PCA
razer = temp(1:36,:);

for i = 1:36

    % distance for Razer
    rHHatX = razer(i,1) - maxXR;
    rHHatY = razer(i,2) - maxYR;
    rHHatZ = razer(i,3) - maxZR;
    rHhatMag = abs(sqrt(rHHatX^2 + rHHatY^2 + rHHatZ^2));

    rHHat = [rHHatX rHHatY rHHatZ];
    rLDot = abs(dot(uHatR,rHHat));

    razerDistances(1,i) = sqrt((rHhatMag^2) - (rLDot^2));
end

```